Spring 4-28-2021

Effect of Precise Control of Crosslink Density on the Thermal, Mechanical, and Conductive Properties of Covalently Crosslinked Ionene Networks

Alexander Thome

Murray State University Honors College

HONORS THESIS

Certificate of Approval

EFFECT OF PRECISE CONTROL OF CROSSLINK DENSITY ON THE THERMAL, MECHANICAL, AND CONDUCTIVE PROPERTIES OF COVALENTLY CROSSLINKED IONENE NETWORKS

Alexander F. Thome

May 8th, 2021

Approved to fulfill the
requirements of HON 437

_____
Dr. Kevin Miller, Professor
Department of Chemistry

Approved to fulfill the
Honors Thesis requirement
of the Murray State Honors
Diploma

_____
Dr. Warren Edminster, Executive Director
Honors College

Examination Approval Page

Author: Alexander F. Thome

Project Title: Effect of Precise Control of Crosslink Density on the Thermal, Mechanical, and Conductive Properties of Covalently Crosslinked Ionene Networks

Department: Chemistry

Date of Defense: April 28th, 2021

Approval by Examining Committee:

_____ _____
Dr. Kevin Miller, Advisor (Date)

_____ _____
Dr. R. Daniel Johnson, Committee Member (Date)

_____ _____
Dr. J. Ricky Cox, Committee Member (Date)

EFFECT OF PRECISE CONTROL OF CROSSLINK DENSITY ON THE THERMAL, MECHANICAL, AND CONDUCTIVE PROPERTIES OF COVALENTLY CROSSLINKED IONENE NETWORKS

Submitted in partial fulfillment

of the requirements

for the Murray State University Honors Diploma

Alexander F. Thome

May 8th, 2021

Table of Contents

List of Figures

List of Schemes

List of Tables

Abstract

Ionic liquids (ILs), besides being well known as environmentally friendly solvents, have attracted attention for a wide variety of other applications, including gas separation, 3D-printing and electrochemical actuators. However, for many such applications, incorporation of the IL moiety into a polymeric material eliminates the use of mechanically unstable free ILs while maintaining many of their electrochemical benefits. Such polymers can take two basic forms: poly(ionic liquid)s are ion-containing polymers in which the IL group is attached pendant to the polymeric backbone, while ionenes are ion-containing polymers in which the IL group is anchored directly into the backbone of the repeating unit. While incorporation into a polymer network inherently reduces ion mobility and thus leads to a decrease in conductivity, particularly in a covalently crosslinked polymer network, polymer architecture can be modified to maximize conductivity. The following experiments attempt to determine specific nanostructural parameters that govern the conductivities of imidazolium-containing ionene networks.

In this thesis, different imidazolium-containing monomers were synthesized by adding alkenyl linkers to an imidazole ring in order to correlate structural variation with polymer properties anion exchange to incorporate the bulky bistriflimide anion, which has been demonstrated in the literature to yield high conductivities relative to other anions. These monomers were incorporated into a covalently crosslinked ionene framework using thiol-ene photopolymerization. The crosslink density was controlled using two synthetic variations: the length of the alkenyl group on the original imidazolium-containing ene monomer, and the thiol:ene functional group ratio. In general, networks in which a stoichiometric thiol:ene functional group

ratio was employed provided the highest gel fractions, thermal stabilities, glass transition temperatures (T_g's), and crosslink densities. They also exhibited the lowest anhydrous ionic conductivities.

A combination of increasing the chain length of the ene monomer and a thiol:ene functional group ratio in which excess ene was utilized provided the highest ionic conductivities (~10^{-5} S/m at 30 °C). This trend of higher conductivity based on increased chain length of the ene monomer did not hold at high temperatures, though; above 50°C, the trend inverts, and the ionene networks with shorter chain lengths had higher conductivities. Moreover, incorporation of a second imidazolium ring in the ene monomer resulted in the highest observed conductivity.

These data suggest two conclusions. The first is that lower T_g values and high ion densities both contribute to an increase in conductivity. The second is that at low temperatures, T_g (polymer flexibility) is the controlling factor, whereas at high temperatures, at which presumably the thermal energy and thus polymer flexibility is high enough to support sufficient conduction for all networks, the ion density is the controlling factor (spatial ion clustering). The unlocking of this fascinating set of competing trends will lend guidance to future studies of related ionene networks. Overall, this thesis will demonstrate that, with precise control of the network architecture, that the thermal, mechanical and conductive properties can be appropriately tuned.

Chapter 1: Introduction

1.1. Ionic Liquids (ILs):

Research concerning ionic liquids (ILs) has ballooned over the last two decades, as the number of applications for them has grown in the literature.[1-4] But what is an ionic liquid? A chemist who uses the term 'ionic' is typically referring to a salt like sodium chloride, a solid crystal in which the cation and anion are so strongly coordinated that they maintain a crystal lattice even at high temperatures. However, more weakly coordinated ions, such as certain salts of bulky organic ions, tend to melt at relatively low temperatures. Those that melt at temperatures lower than 100°C are defined as ionic liquids (ILs), and those that are liquid at room temperature are defined as room temperature ionic liquids (RTILs).

There are a few organic cations commonly associated with ILs. Shown in Figure 1.1 are eight examples: tetraalkylammonium, pyrrolidinium, imidazolium, 1,2,3-triazolium, pyridinium, phosphonium, and trialkylsulfonium. The various properties of these cations and their derivatives, combined with the large number of anions with which they can be paired, leads to a great landscape of possible properties for ILs.[2, 4, 5] The chemical structures of a few common anions are displayed in Figure 1.2, including bis(trifluoromethane)sulfonimide ("bistriflimide"), triflate, hexafluorophosphate, tetrafluoroborate, and perchlorate.

Preparation of ILs can be challenging. Impurities can come from starting materials or flasks used, and they are hard to remove due to the difficulty of distilling ILs in bulk.[6] In addition, the first step is typically an alkylation that occurs via nucleophilic substitution and forms the organic cation, a step which is highly exothermic and can lead to a runaway reaction, ruining the synthesis. For this reason, this step of the reaction is commonly performed in solution at low heat.[1] It is the

present authors' personal experience that simply adding the nucleophile and the electrophile to the flask together before the solvent is added can be enough to cause the reaction mixture to overheat. Some success has been found in the literature in preventing the formation of hot spots in the reaction mixture by microwave or ultrasound radiation.[1] Moreover, in IL synthesis this first step usually produces an organic halide salt, which may be an IL but is typically not a RTIL; this material may thus be recrystallized to maximize purity, most commonly in acetonitrile, with ethyl acetate sometimes serving as a precipitating agent.[1] The solid IL may then be converted to a number of other ILs via an anion exchange reaction with a metal or an ammonium salt of the desired anion.

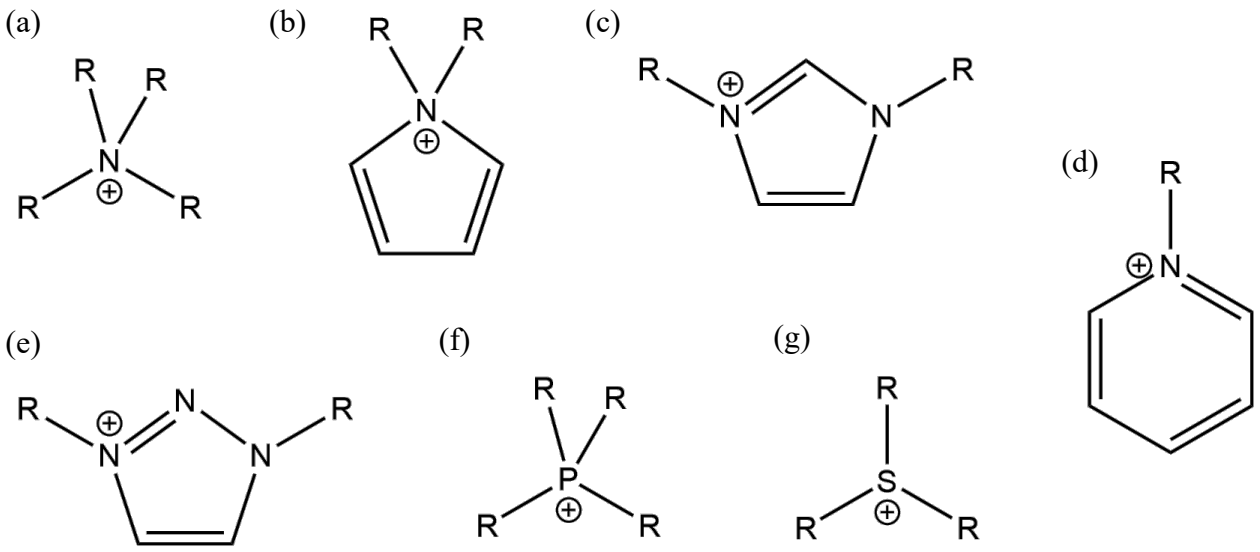

Figure 1.1. Chemical structures of common ionic liquid cations: pictured here are tetraalkylammonium (a), pyrrolidinium (b), imidazolium (c), pyridinium (d), 1,2,3-triazolium (e), phosphonium (f), and trialkylsulfonium (g).

The applications for which ILs have so far been investigated are most commonly centered around synthesis and catalysis for their advantages as solvents.[1, 4] One of the most important properties of a solvent is polarity. The old cliché that 'like dissolves like' is quite true, and in order to serve as a viable solvent for a given synthesis, an IL needs to have a similar polarity to the reagents that need to dissolve. Formally, polarity is the sum of all possible interactions between the solvent and any potential solute, excluding those related to chemical reactions.[1] A quantitative measure of this interpretation of polarity is the IL's dielectric constant, which can be widely referenced for common solvents as well as those that have been moderately studied. For ammonium- and imidazolium-based ILs, the literature has shown that the dielectric constant decreases with increasing basicity of the anion.[1] Moreover, the dielectric constant decreased when the cations' alkyl chain length increased, an intuitive result given that increasing the length of the alkyl chains decreases ion density.

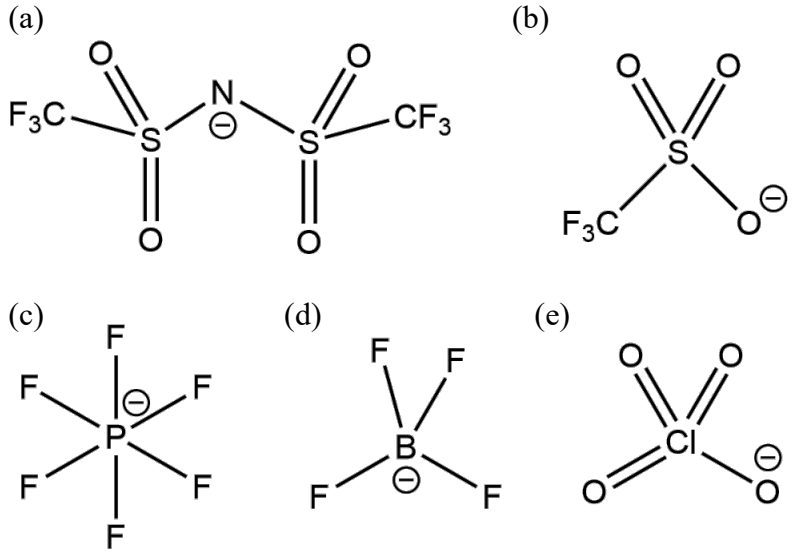

Figure 1.2. Chemical structures of common ionic liquid anions: pictured here are bis(trifluoromethane)sulfonimide ("bistriflimide") (a), triflate (b), hexafluorophosphate (c), tetrafluoroborate (d), and perchlorate (e).

Additionally, ILs have been investigated for applications in gas separation. However, ILs have proved not to be the best candidate for gas separation; membranes that include them have poor performance due to ILs' liquid state.[7] Namely, ILs' lack of mechanical stability requires other materials to be designed to encase them and are prone to leaking and other problems. Therefore, gas separation is discussed in more depth in the following section as related to IL-based polymers, which have proved to be much better candidates that can combine the desirable properties of ILs as well as the mechanical stability of a viscoelastic polymer. Further applications of ILs include 3D printing[8, 9] and electroactive devices.[10-12]

1.2. Poly(Ionic Liquid)s (PILs) and Ionenes

Incorporation of an IL into a polymer seeks to combine advantageous properties of polymer systems, such as mechanical stability, processability, and viscoelasticity, with the desirable properties of ILs; namely ionic conductivity, thermal stability, and electrochemical stability. This is an ongoing challenge, due to a number of difficulties inherent in preserving the best of both worlds. One example is that anchoring an IL to a polymer chain decreases ion mobility, lowering the ionic conductivity of an IL-containing polymer by about two orders of magnitude with respect to the corresponding IL.[7] However, research has been steadily unlocking the relationships between structure and properties of IL-containing polymers, a field of study which is briefly introduced below.

When an ionic liquid moiety is incorporated into a polymer, the resulting architecture is classified in terms of two main forms: the ionic species can be tethered to the main chain in a pendant fashion, or they can be linked within the main chain. The former are referred to as poly(ionic liquid)s, and the latter as ionenes, and an illustration of each is shown in Figure 1.3.

Due to the similar range of properties and of applications for which poly(ionic liquid)s and ionenes are being investigated, this distinction is not strictly followed in the literature, particularly in the broader application of term 'poly(ionic liquid)' to include polymers that fit the definition of ionene. Therefore, while the terms will be kept separate in this work, readers should be aware that of their looser use in the literature, and that many times when this work refers to another author's study of a selection of ionenes, the referenced paper uses term PIL.

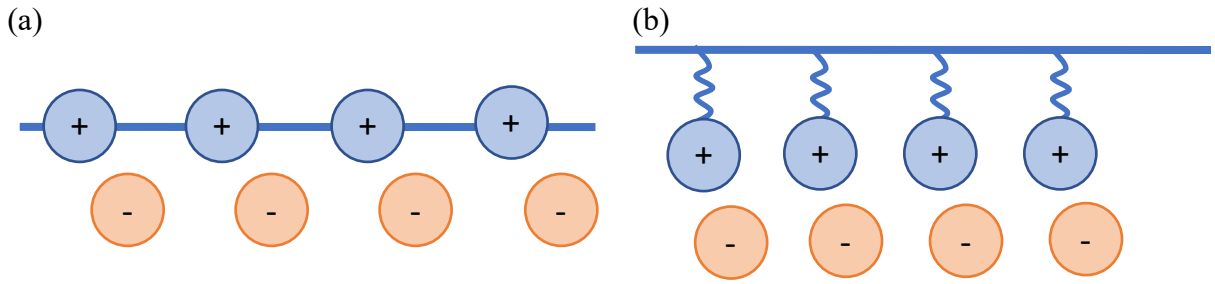

Figure 1.3. Sketches of the skeletal structures of a cationic ionene (a), and a cationic poly(ionic liquid) (b). The solid blue line represents the polymer backbone.

Poly(ionic liquid)s, abbreviated as PILs and sometimes referred to as polyelectrolytes, typically resemble common polymers with an IL moiety tethered to a certain place. Examples, shown in Scheme 1.1, include a vinylimidazolium polymer, which is a modified polyethylene at heart, and a sulfonate polymers shown next to them are a modified polystyrene. Additionally, acrylate derivatives are another common backbone type, and copolymers that include IL monomers combined with nonionic monomers have also been studied.[7] As the Figure 1.3 implies, the pendant ions can carry positive or negative charge, with a 'free' counterion of the opposite charge paired with each one, although pendant cations are far more common due to their synthesis

being easier.[13] Still, anionic PILs that have been investigated have been found to have high ionic conductivities relative to cationic counterparts.[14]

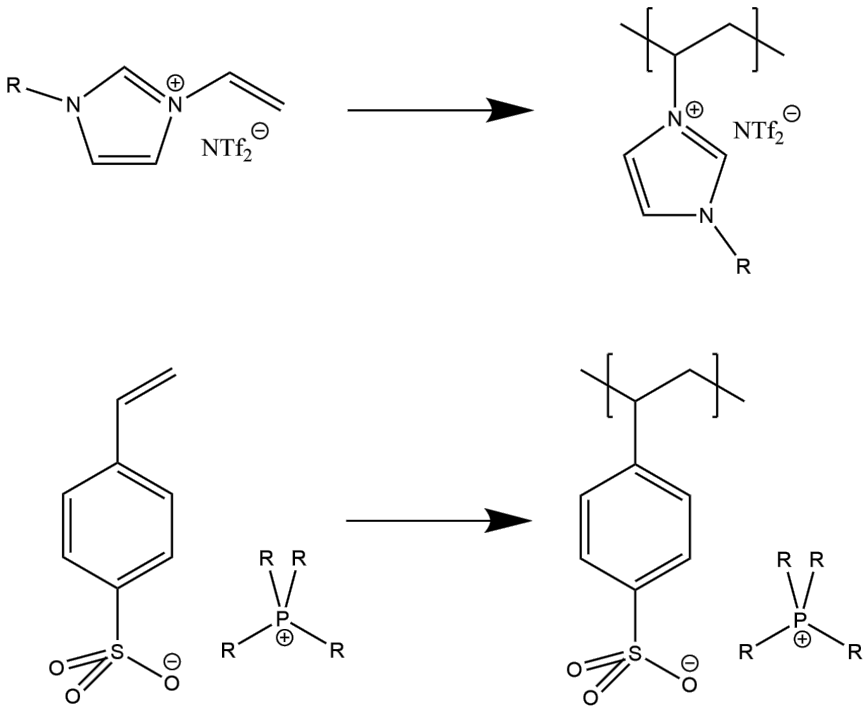

Scheme 1.1. Chemical structures and polymerization of some example PIL monomers (a) poly(vinylimidazolium bistriflimide) and (b) poly(tetraalkylphosphonium styrene sulfonate)

Ionenes are the subject of a recent review by Bara et al.[13] Their survey of the literature finds that most ionene syntheses take place via a Menshutkin reaction between tertiary diamines and α, ω-dihaloalkanes. An illustration of this reaction is shown in Scheme 1.2. Other cations, such as *N*-heterocyclic cations and phosphonium (See Figure 1.1) have been used in similar syntheses, as well as xylyl and ether linkages between IL groups. As with PILs, both cationic and anionic ionenes are both possible, with the same caveat that anionic ionenes are more difficult to synthesize. However, anionic ionenes may have advantages that make surmounting these

difficulties worthwhile, including improved thermal stability as well as the ability to contain reactive/catalytic cations, such as hydrogen and metal ions.[13]

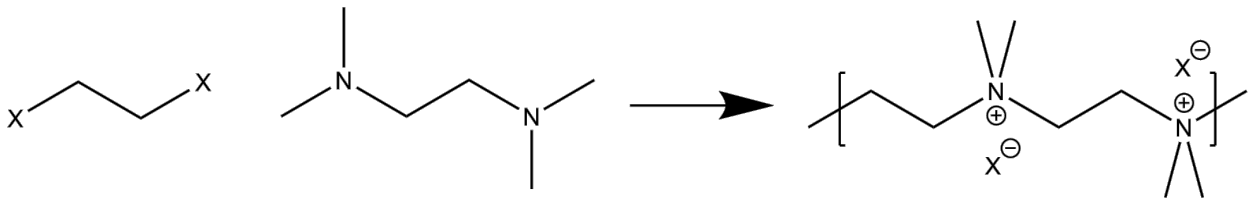

Scheme 1.2. The Menshutkin reaction: nucleophilic substitution of the halides by the lone pair of electrons on each nitrogen leads to a coupling that results in a tetraalkylammonium moiety. The molecules in question polymerize because they are both bifunctional.

Among the significant applications of both PILs and ionenes is gas separation.[15-20] In particular, imidazolium-based PILs have shown high CO_2 absorption capacities, and importantly, they are selective to CO_2 above H_2, N_2, and O_2.[17-19] The bistriflimide anion has a particularly high affinity for CO_2.[20] PIL or ionene membranes could thus serve an important role in carbon capture from flue gas streams, along with other potential related uses. Anion exchange membranes are another place that PILs and ionenes find a use;[21] such a membrane could alternatively be reshaped as a cation exchange membrane by using an anionic PIL or an anionic ionene.[13] Additionally, PILs and ionenes have made attracted interest in their own right for potential applications in 3D-printing[22, 23] and electroactive devices.[24, 25] Further commonly studied applications include microwave-absorbing transparent materials for microwave ovens[26] and drug delivery.[27, 28]

1.3. Thiol-ene Chemistry

In a 2001 review,[29] the prolific organic chemist and later Nobel laureate K. Barry Sharpless coined the term 'click chemistry.' Sharpless meant the term to refer to selective reactions that rely on heteroatom links rather than formation of new carbon-carbon bonds, which can involve difficult and costly synthetic procedures. To fit the definition of a click reaction, a given reaction must also be modular, wide in scope, and deliver high yields, as well as forming only 'inoffensive' by-products that can be removed without chromatography and being able to be run under simple reaction conditions. The term 'click' is used because such reactions tend to have a large thermodynamic force driving them, and thus be metaphorically spring-loaded for a single reaction pathway.[29]

The thiol-ene reaction is one such click reaction.[30] It is a radical coupling of a thiol (-SH) functional group and an alkene (C=C) to form a thioether linkage (C-S-C), as shown in Scheme 1.3 with an illustration of the reaction mechanism. In addition to meeting the requirements of being a click reaction, it is also photoinitiated, which allows for spatial and temporal control of the reaction. The authors who characterize it as a click reaction note that it is excellent for producing highly uniform polymer networks.[30] In the initiation step, the photoinitiator forms a radical upon the exposure to ultraviolet light, and it abstracts a hydrogen radical from the thiol, leaving a thiol radical. Propagation happens when the sulfur radical reacts with an alkene, forming the new C-S-C linkage as well as creating a carbon radical. A chain transfer propagation step happens when the carbon radical abstracts a hydrogen radical from another thiol group, creating a new thiol radical. Termination happens when two thiols form an S-S bond, a thiol radical forms a new bond with a carbon (formerly an ene carbon) radical, or two carbon radicals join together.

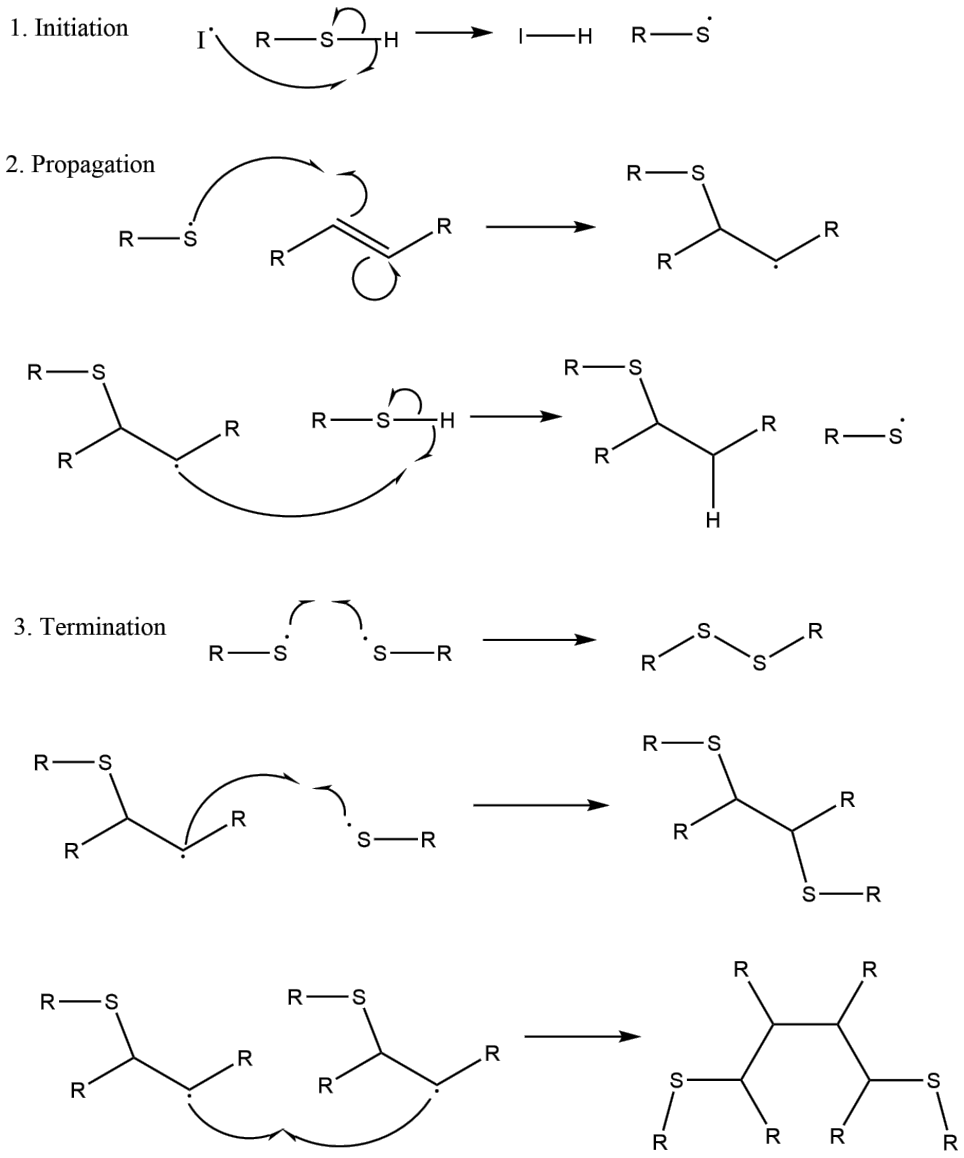

Scheme 1.3. Mechanism of the thiol-ene ‘click’ reaction

Thiol-ene photopolymer networks are therefore attractive for their ease of synthesis. A number of examples of their use in ionene research are detailed in the next section, and two interesting additional examples are explored below. In a study published in 2017, Tibbits et al. used thiol-ene chemistry to synthesize poly(ionic liquid) networks with high conversions and good uniformity.[31] Interestingly, they found that exchange of the bromide anion for the bistriflimide

anion (see Figure 1.2) caused both a decrease in glass transition temperature and in ionic conductivity. In a 2020 paper, Long et al. used thiol-ene chemistry for the purpose of joining two types of polymers together into a series of graft copolymers.[32] Specifically, they designed uniform water soluble graft copolymers which has potential applications in binder jetting additive manufacturing, a 3D-printing process.

1.4. Previous Miller Group Work

The Miller research group has studied poly(ionic liquid) (PILs) and ionene networks for nearly a decade at Murray State University. Previous work has employed a variety of synthetic techniques, including Michael addition[33-35] and thiol-ene chemistry,[36-38] as well as a variety of ionic liquid (IL) species, including imidazolium,[36, 37] 1,2,3-triazolium,[34, 35] and phosphonium salts,[38] (see Figure 1.1) to form covalently crosslinked polymer networks that contain IL moieties. In the course of these works, various trends have been established in the thermal, mechanical, and conductive properties of the networks synthesized, some of which are detailed below.

Among the first efforts in the Miller group to synthesize ionene networks was a 2012 study by Kim et al., in which imidazolium-containing polyesters were polymerized via a Michael addition reaction.[33] The authors studied the effect of different counteranions on the glass transition temperature (T_g) and thermal stability, as defined by the temperature at which five-percent of the material has decomposed ($T_{d5\%}$), of their respective networks. They found that larger anions produced networks with the lower T_g, and that in general, more basic anions produced networks with lower thermal stability. The bistriflimide anion (see Figure 1.2) was both the largest and the least basic of the anions studied, giving the bistriflimide network the lowest T_g and the highest thermal stability. This is result similar to the results of experiments by Long et al., in which an

imidazolium containing linear PIL experienced a decrease in T_g and an increase in ionic conductivity as the anion became bulkier.[39]

Thiol-ene chemistry was first used in the polymerization of ionene networks as reported in 2016 by Rhoades et al.[37] That study employed the same tetrafunctional thiol as this study, pentaerythritol tetrakis(3-mercaptopropionate) ("PTMP"), as well as one of the same difunctional ene IL monomers (bisallylimidazolium bistriflimide), both shown in Figure 1.4. The authors explored the effect of varying the molar ratios of thiol to ene. It was found that the stoichiometric ratio (1.0:2.0 thiol:ene) yielded an ionene network with the highest T_g, highest $T_{d5\%}$, and highest crosslink density, and the lowest ionic conductivity. However, while the ionic conductivity of each of the polymers was inversely correlated with T_g, the curves did not collapse on one another when normalized with respect to T_g, implying other factors that control the conductivity. The authors suggest that ion density may be another factor, since the T_g-normalized conductivities increase with increasing ratio of IL ene monomer.

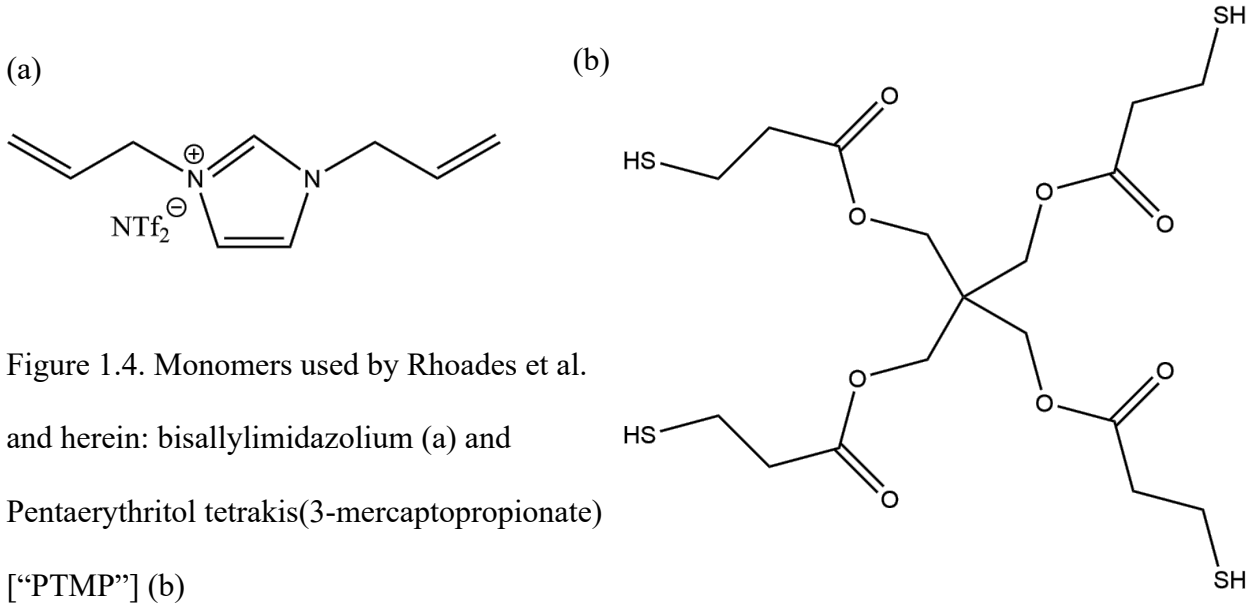

Figure 1.4. Monomers used by Rhoades et al. and herein: bisallylimidazolium (a) and Pentaerythritol tetrakis(3-mercaptopropionate) ["PTMP"] (b)

In 2018, Bratton et al. published a study that continued the work of Rhoades et al,, in which they examined the effect of adding monofunctional IL ene monomers, which become pendant IL functional groups, on the thermal, mechanical, and conductive properties of the resulting networks.[36] Some of these monofunctional IL ene monomers had variable alkyl chains attached, and some had variable alkyl tethers. It was found that longer alkyl tethers resulted in lower T_g's, lower storage moduli (E'), and higher conductivity, while longer attached alkyl chains led to a similar result up to a limit of eight carbons, after which adding more carbon atoms to the alkyl chain increased T_g and decreased conductivity. The authors postulate that this effect is observed due to extended crystallinities that form in the network, due to interdigitation of the alkyl chains. They support this explanation with XRS data; a scattering peak assigned to the backbone-backbone correlation distance is seen for sixteen and twenty carbon chains which disappears above the melting temperature, strongly suggestive of extended crystallinities.

Thiol-ene chemistry was also employed in the synthesis of phosphonium-based ionene networks by Sims et al. in a study published in 2019.[38] The results are similar to the previous imidazolium-based studies, in that more flexible chains had lower T_g's and higher ionic conductivities as a result. Additionally, while the phosphonium-containing monomers exhibited high thermal stabilities relative to imidazolium-containing analogues, the resulting ionene networks saw no significant improvement, due to a two-step decomposition that begins at a temperature similar to that of imidazolium-based ionene networks.

1.5. Purpose

This study seeks to build on the work of Rhoades et al. and Bratton et al., and establish a more comprehensive correlation between variables in the polymer architecture and

thermomechanical and conductive properties. Specifically, a correlation between crosslink density, as controlled by varying the length of alkyl spacers between crosslink points and the ratio of tetrafunctional thiol monomer and difuctional IL ene monomer, and properties of the polymer network. These properties include glass transition temperature (T_g), thermal stability (as measured by $T_{d5\%}$), storage modulus (E'), and the ionic conductivity. Trends in ionic conductivity will be explored in the context of X-ray scattering (XRS) data, which will provide clues that may give added clarity to the precise factors that influence ionic conductivity.

Chapter 2: Results and Discussion

2.1. IL Monomers - Synthesis and Characterization

Monomer synthesis was accomplished in two related synthetic pathways. Scheme 2.1 shows the steps used for the first three monomers, all of which are mono-imidazolium containing and are henceforth denoted by their alkenyl linking branches: “allyl,” “hexenyl,” and “decenyl” as shown. The first step of this synthesis was the addition of the appropriate bromoalkene to a small excess of sodium imidazole in refluxing tetrahydrofuran. After purifying this monosubstituted imidazole product, which took place by column chromatography in the case of the hexenyl and decenyl monomers, a small excess of the same alkenyl linker was added to it in a solution of acetonitrile at 60°C. The final step of the synthesis involved anion metathesis for the bulkier bistriflimide anion, which is preferred for conductivity applications.[33, 39] This took place by dissolving the bromide IL along with lithium bistriflimide in water; the bistriflimide ILs are insoluble in water, and thus after a few days, the product could be removed by separation of the two resulting phases. Completeness of anion exchange was tested qualitatively, by dissolving product (~ 1 mg) in acetone (~ 1 mL) and adding a milliliter of concentrated aqueous silver nitrate. The absence of silver bromide precipitate demonstrated the absence of bromide ions in the product.

The second synthetic pathway, shown in Scheme 2.2 is only slightly modified from the first; the first step is accomplished by more than two equivalents of sodium imidazole to 1,6-dibromohexane, the excess being necessary to avoid products like those of the Menshutkin reaction (see Scheme 1.2), forming a bisimidazole-substituted product. The remaining reagents, including allyl linkers, were added in excess of two equivalents, in order to react with both imidazolium substituents. This monomer is denoted the “bisimidazolium” monomer for future reference.

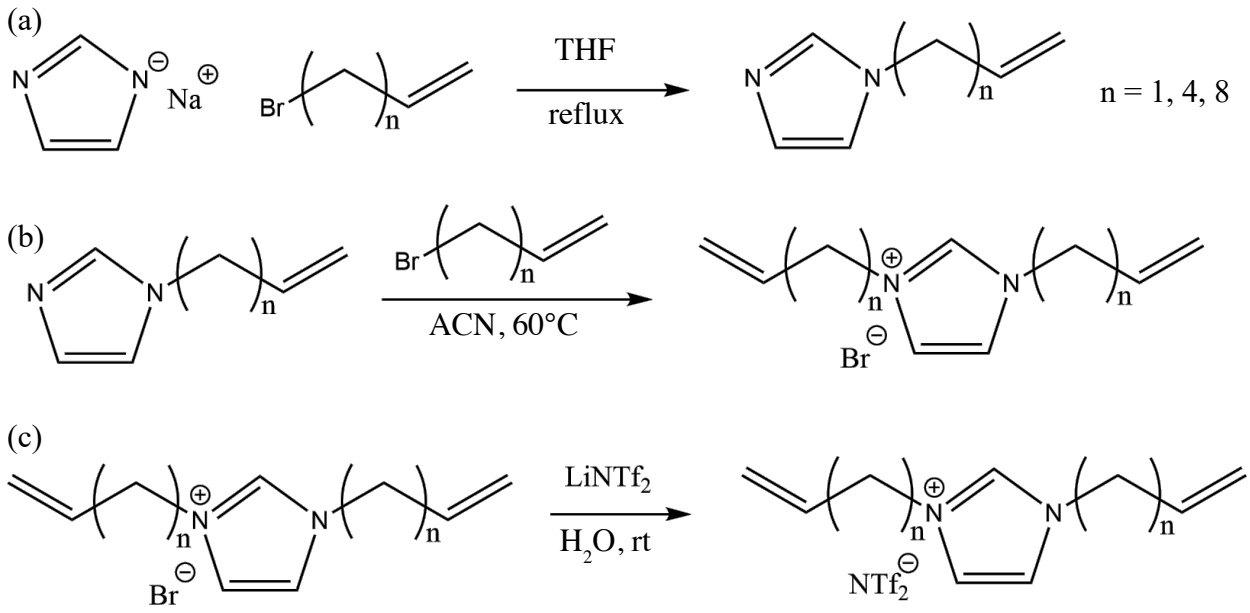

Scheme 2.1. Synthetic method for the allyl (n = 1), hexenyl (n = 4), decenyl (n = 8) monomers. This was accomplished in three steps: monoaddition of one alkene linker to the imidazolium ring (a), second addition of an alkene linker to form a bromide ionic liquid (b), and anion metathesis to replace the bromide anion with bistriflimide (c).

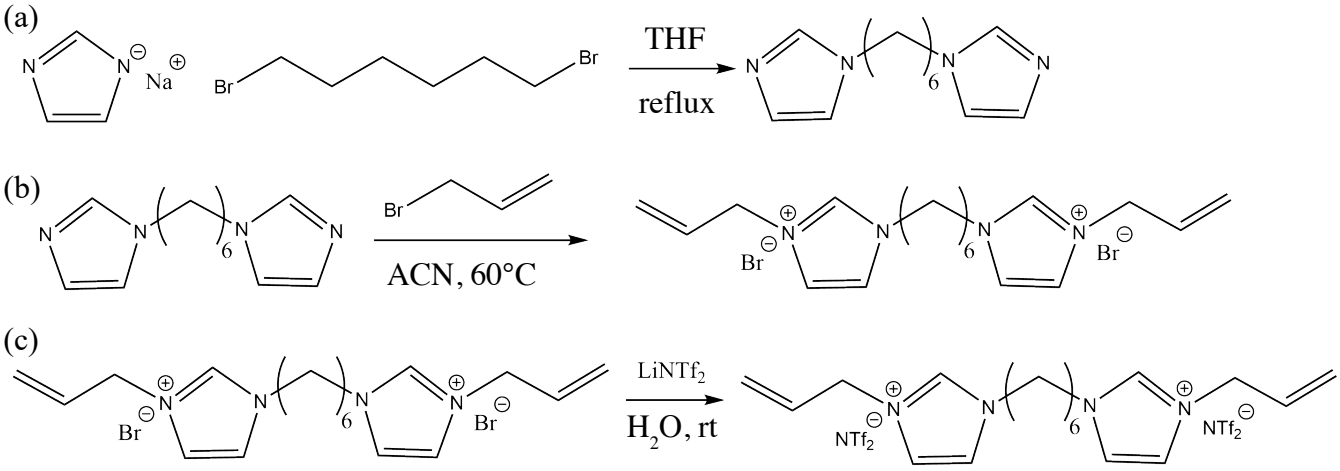

Scheme 2.2. Synthetic method for the bisimidazolium monomer. This was accomplished in three steps: addition of two imidazolium rings to the 6-carbon chain via a Menshutkin-like reaction (a), addition two allyl linkers to form a dibromide ionic liquid (b), and anion metathesis to replace both bromide anions with bistriflimide (c).

Synthetic yields for the first step (monosubstitution) were approximately 70% for each system. The second step (second alkene addition) had a yield of 88% for the hexenyl synthesis,[40] 77% for the decenyl synthesis (both of which are calculated after purification by column chromatography), and 84% for the bisimidazolium synthesis. The final step (anion metathesis) had a yield of about 94% for each synthesis except for the decenyl IL monomer, which was 83% The monomers were characterized by nuclear magnetic resonance (NMR) spectroscopy. Proton NMR (^{1}H-NMR) spectra were recorded for all synthetic products; decenylimidazole, as well as the bromide and bistriflimide ILs of the decenyl and bisimidazolium monomers, were additionally characterized by carbon NMR (^{13}C-NMR) spectroscopy. A sample ^{1}H-NMR spectrum with assignments is shown in Figure 2.1; more spectra are included in the Appendix, Figures A1-A11.

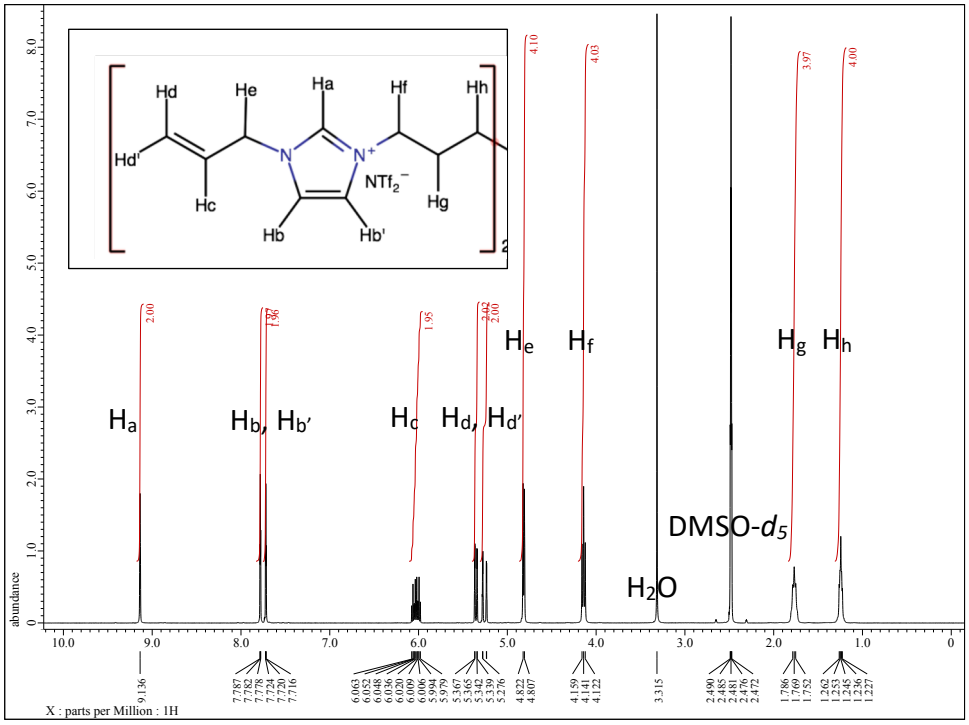

Figure 2.1. ^{1}H-NMR spectrum (DMSO-d_6) of hexane-1,6-bis(3-allylimidazolium bistriflimide) with assignments.

2.2. Ionene Synthesis and Characterization

Synthesis of the polymer networks took place by adding each of the four respective IL monomers described above to a specific molar ratio of a tetrafunctional thiol (pentaerythritol tetrakis(3-mercaptopropionate), "PTMP") and a small amount of photoinitiator (1 wt%). This mixture was irradiated with UV light to initiate the thiol-ene 'click' reaction (see Section 1.4), and the cured polymer networks were dried in a vacuum oven (24 h, 60°C, <0.1 mmHg) prior to further analysis. Polymer networks were prepared at thiol:ene molar ratios of 1:1, 1:2 (stoichiometric), and 1:3 for each of the four IL monomers; the resulting films were a transparent brownish yellow in color, and the color intensity increased with increasing molar ratios of IL. The synthesis is briefly outlined in Scheme 2.3.

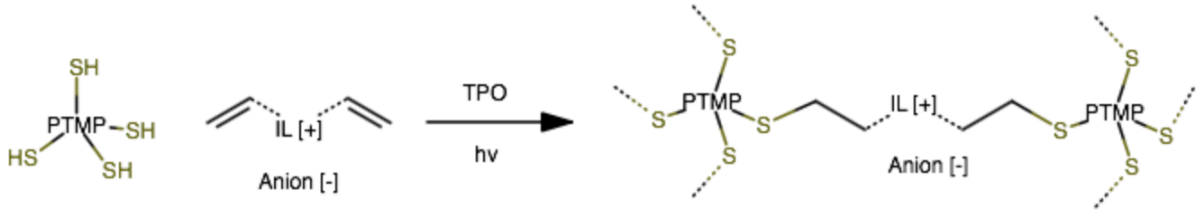

Scheme 2.3. Polymer synthesis procedure: photopolymerization of the tetrafunctional thiol (PTMP, see Figure 1.4) with an IL bifunctional 'ene' monomer. This synthesis was carried out at thiol:ene molar ratios of 1:1, 1:2, and 1:3.

Each of the polymer networks was analyzed by gel fraction analysis, a technique which allows determination of the percentage of monomer incorporated into a crosslinked network (gel). This was performed using a Soxhlet equipped with a cellulose thimble and using THF as the solvent. Results for the decenyl and bisimidazolium networks are shown in Table 2.1. It can readily be seen that for a given IL monomer, the stoichiometric (1:2) polymer networks had a higher gel

fraction than their non-stoichiometric counterparts (1:1 and 1:3), as would be expected due to the 1:2 network having an equal number of thiol and ene functional groups. The exception is the high gel fraction of the 1:1 bisimidazolium network; this result seems anomalous, but because no work has been done on closely related bisimidazolium-containing ionene networks to date, more investigation is necessary to determine whether this result is an experimental error or indicative of a broader trend.

Table 2.1: Gel Fraction Data of Imidazolium Polymer Networks

IL monomer	Thiol:ene molar ratio	% Swelling	Gel Fraction
Allyl	1.0:1.0	161 ± 22 %	77.0 ± 0.5 %
Allyl	1.0:2.0	146 ± 4 %	99.7 ± 0.1 %
Allyl	1.0:3.0	135 ± 7 %	74.7 ± 1.0 %
Hexenyl	1.0:1.0	178 ± 6 %	81.5 ± 1.0 %
Hexenyl	1.0:2.0	149.8 ± 0.5 %	98.5 ± 0.2 %
Hexenyl	1.0:3.0	160.3 ± 0.9 %	79.5 ± 0.5 %
Decenyl	1.0:1.0	173 ± 4 %	93.5 ± 2.4 %
Decenyl	1.0:2.0	154 ± 7 %	96.9 ± 0.4 %
Decenyl	1.0:3.0	174 ± 3 %	81.2 ± 0.3 %
Bisimidazolium	1.0:1.0	158.6 ± 0.4 %	96.4 ± 0.8 %
Bisimidazolium	1.0:2.0	142.6 ± 0.6 %	93.6 ± 0.5 %
Bisimidazolium	1.0:3.0	127 ± 2 %	70.9 ± 1.8 %

Additionally, the allyl and bisimidazolium networks showed a trend in swollen mass of 1:1 > 1:2 > 1:3, in agreement with previous results for allyl networks,[37] while the hexenyl and decenyl networks had significantly lower swollen masses for 1:2 than for either of non-stoichiometric networks (1:2 << 1:1, 1:3). The underlying causes that distinguish these trends are not completely understood from these data; theoretically, the percent swelling that a polymer network exhibits is

inversely proportional to the crosslink density. However, the trend in crosslink density by thiol:ene molar ratio is 1:2 >> 1:3 > 1:1 for all of the networks, as demonstrated by mechanical analysis (see Section 2.3), which is the intuitive result. Future work may be needed to understand the reasons behind this unusual trend for the allyl and bisimidazolium networks.

2.3. Thermal and Mechanical Analysis

Thermal analysis was carried out via TGA and DSC measurements on each of the polymer networks. The results of these experiments are shown in Table 2.2. For each of the polymer networks, the trend in thermal stability, as measured by the temperature at which the mass has decreased five percent from the initial mass in a TGA experiment ($T_{d5\%}$), is 1:2 > 1:3 > 1:1 for a given IL monomer.

Table 2.2: Thermal Analysis of Imidazolium Polymer Networks

IL monomer	Thiol:ene molar ratio	$T_{d5\%}$ (°C)	DSC T_g (°C)
Allyl	1.0:1.0	344[37]	-25.2
Allyl	1.0:2.0	346[37]	-13.6
Allyl	1.0:3.0	349[37]	-30.2
Hexenyl	1.0:1.0	3345	-33.8
Hexenyl	1.0:2.0	3556	-20.0
Hexenyl	1.0:3.0	346	-40.8
Decenyl	1.0:1.0	-	-34.8
Decenyl	1.0:2.0	361	-23.0
Decenyl	1.0:3.0	348	-40.9
Bisimidazolium	1.0:1.0	344	-29.5
Bisimidazolium	1.0:2.0	353	-24.0
Bisimidazolium	1.0:3.0	349	-38.1

The trend in T_g as measured in DSC experiments by thiol:ene molar ratio follows the sequence 1:2 > 1:1 > 1:3, for a given IL monomer. The trend in T_g by monomer is allyl > hexenyl > decenyl, which correlates with backbone chain flexibility. However, it is probable that this trend does not hold for indefinitely higher numbers of carbon atoms in the alkyl linkers; the work of Bratton et al. found an increase in T_g when enough carbon atoms (between eight and twelve) were present as pendant chains, they caused semicrystalline regions to form, in which interdigitation of alkyl chains led to increased rigidity and increased T_g.[36]

It is worth noting that the overall length of the bisimidazolium monomer is comparable to that of the hexenyl monomer, and this similarity in polymer architecture that probably leads to their similar T_g values. However, as a whole the bisimidazolium networks do not fall neatly into the trends in thermal properties found for the other ionene networks studied. while the trend by thiol:ene molar ratio still holds, the 1:2 bisimidazolium network has the lowest T_g compared to all of the 1:2 networks, but the 1:1 and 1:3 bisimidazolium networks have a higher T_g than both the hexenyl and decenyl counterparts. In a sense, the thiol:ene molar ratio trend in T_g of 1:2 > 1:1 > 1:3 still holds, there is a smaller difference than in any of the monoimidazolium networks, or a 'gentler' trend. Because no work has been done on closely related bisimidazolium-containing ionene networks to date, more investigation will have to be done to determine the exact trends.

Mechanical properties as measured in DMA experiments are shown in Table 2.3. Trends in mechanical strength are evaluated by comparing the storage modulus (E') at a specific temperature (100°C) in the rubbery plateau of the DMA curve ($T >> T_g$) for each of the networks. It is clear from these data that for a given IL monomer, the trend in relative mechanical strengths based on thiol:ene molar ratio is 1:2 >> 1:3 > 1:1. This is an intuitive result, because the crosslink density, which is theoretically proportional to E' and is calculated from that value, is expected to

be higher for the networks with an equal ratio of thiol and ene functional groups (1:2 networks) than for those with unequal ratios (1:1 and 1:3 networks). Crosslink densities were calculated from the equation below:

$$\rho_x = \frac{E'}{3RT}$$

Table 2.3: Mechanical Properties of Imidazolium Polymer Networks

IL monomer	Thiol:ene molar ratio	E' @ 100°C (MPa)	ρ_x x 10^4 (mol/cm^3)
Allyl	1.0:1.0	0.325	0.349
Allyl	1.0:2.0	6.827	7.335
Allyl	1.0:3.0	0.797	0.856
Hexenyl	1.0:1.0	0.935	1.004
Hexenyl	1.0:2.0	8.964	9.631
Hexenyl	1.0:3.0	1.419	1.524
Decenyl	1.0:1.0	1.225	1.316
Decenyl	1.0:2.0	7.458	8.013
Decenyl	1.0:3.0	1.352	1.452
Bisimidazolium	1.0:1.0	0.351	0.377
Bisimidazolium	1.0:2.0	3.290	3.535
Bisimidazolium	1.0:3.0	0.463	0.497

No meaningful result is observed in the trends in E' with respect to linker chain, except that the value for the 1:2 bisimidazolium network is curiously low in comparison to the other 1:2 networks. Future work on related bisimidazolium-containing ionene networks will shed light on the significance of this result.

2.4. Ionic Conductivities of Ionene Networks

Each of the twelve ionene networks was also evaluated for ionic conductivities by dielectric relaxation spectroscopy (DRS). Briefly, the DC conductivity (σ_{DC}) was determined from the plateau value observed in the real conductivity function ($\sigma' = \omega\varepsilon''\varepsilon_0$, where ω is the frequency, ε" is the dielectric loss, and ε_0 is the vacuum permittivity). These DC conductivity values as a function of temperature were fit to a Vogel-Fulcher-Tammann (VFT) relationship, according to the following equation:

$$\sigma_{DC} = \sigma_{\infty} \times e^{-DT_0/(T-T_0)}$$

in which σ_{∞} is the high temperature upper bound of ionic conductivity, D is a strength parameter related to the ionic conductivity activation energy, and T_0 is the Vogel temperature (at which ionic conductivity diverges to zero). Ionic conductivities for each of the polymer networks, along with fitting parameters, are shown in Table 2.4. Fitted curves plotted against experimental data are shown in Figure 2.2.

It can be clearly seen that, under anhydrous conditions at 30°C, the trend in ionic conductivity by IL monomer for the 1:2 networks is allyl < hexenyl < decenyl < bisimidazolium, and the trend by molar ratio for a given IL monomer is 1:2 < 1:1 < 1:3. With the exception of the bisimidazolium, which is a different type of monomer, this trend follows the trend in glass transition temperature observed in DSC experiments, implying a high T_g-dependence, of the ionic conductivity; in essence, the conductivity has a high dependence on the flexibility of the network. This is further investigated by examining the plots of conductivity [log (σ_{DC})] as a function of T_g/T for the different thiol:ene molar ratios of a given IL monomer. These plots, displayed in Figure 2.3, show some collapse of the curves on each other, which implies a high T_g-dependence.

However, the trend (1:2 < 1:1 < 1:3) is still observable, which implies that there are other factors affecting the conductive properties of these ionene networks.

Table 2.4: Conductivity Data and VFT Fitting Parameters of Imidazolium Polymer Networks

IL monomer	Thiol:ene molar ratio	$\sigma_{DC,30°C}$ (S/cm)	σ_∞ (S/cm)	D	T_0 (K)
Allyl	1.0:1.0	6.9×10^{-6}	1.02	7.6	185.0
Allyl	1.0:2.0	1.1×10^{-6}	0.70 (0.72)*	7.0	198.6
Allyl	1.0:3.0	6.1×10^{-5}	1.47	7.0	178.7
Hexenyl	1.0:1.0	7.9×10^{-6}	0.47	7.4	181.0
Hexenyl	1.0:2.0	1.5×10^{-6}	0.12 (0.32)*	6.5	192.6
Hexenyl	1.0:3.0	3.3×10^{-5}	0.74	8.0	168.5
Decenyl	1.0:1.0	5.7×10^{-6}	0.44	7.9	178.1
Decenyl	1.0:2.0	2.0×10^{-6}	0.14	7.4	182.5
Decenyl	1.0:3.0	2.3×10^{-5}	0.67	8.4	166.3
Bisimidazolium	1.0:1.0	2.5×10^{-5}	1.79	6.8	181.5
Bisimidazolium	1.0:2.0	4.8×10^{-6}	0.72	7.5	186.7
Bisimidazolium	1.0:3.0	6.7×10^{-5}	2.03	7.6	180.8

*Literature values listed in parentheses for select networks.[37, 40]

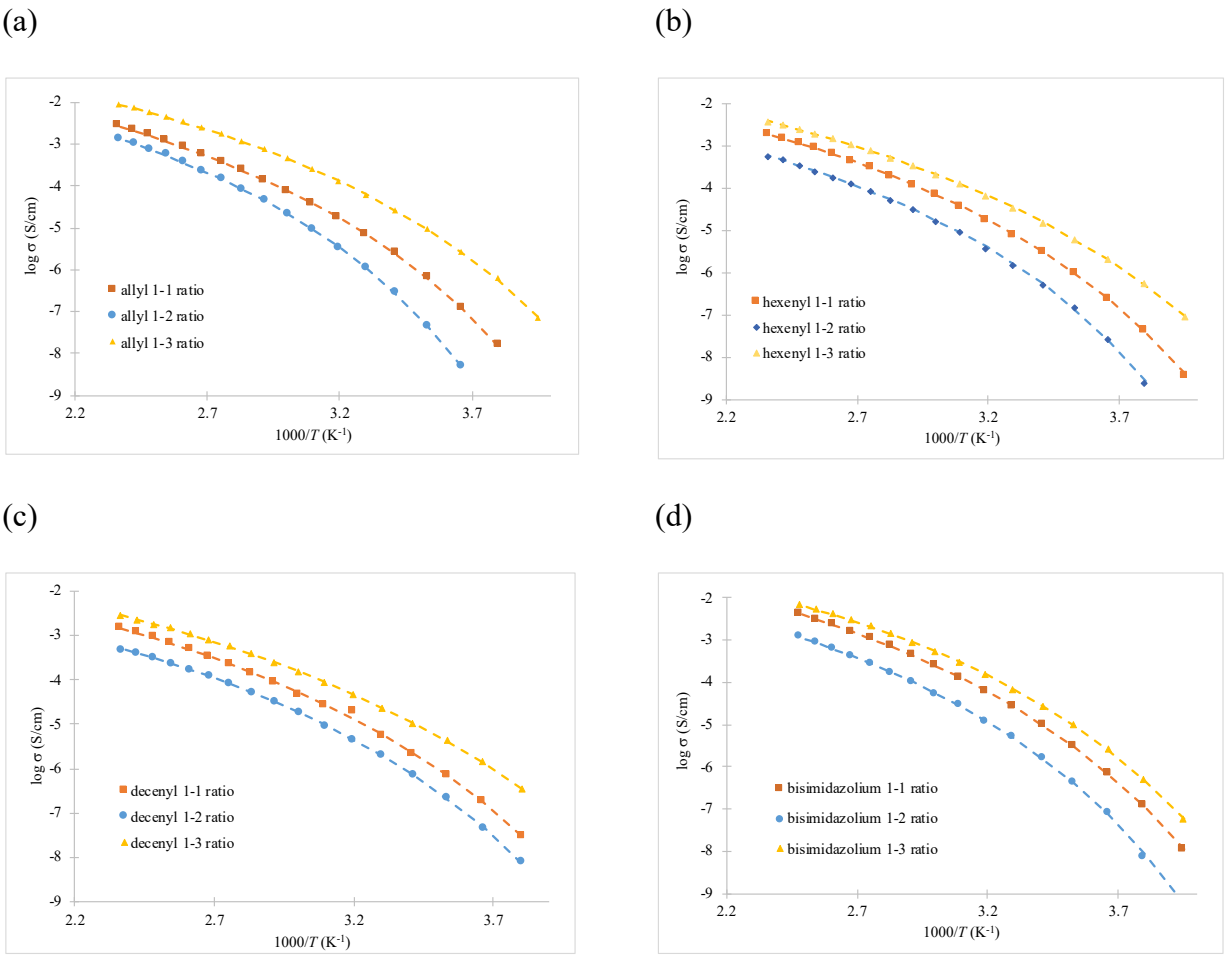

Figure 2.2. Conductivity [expressed in terms of log (σ_{DC})] plotted as a function of temperature [expressed as $1000/T$, where T is the absolute temperature in Kelvin] for the allyl (a), hexenyl (b), decenyl (c), and bisimidazolium (d). Fitted VFT functions are shown in dashed lines.

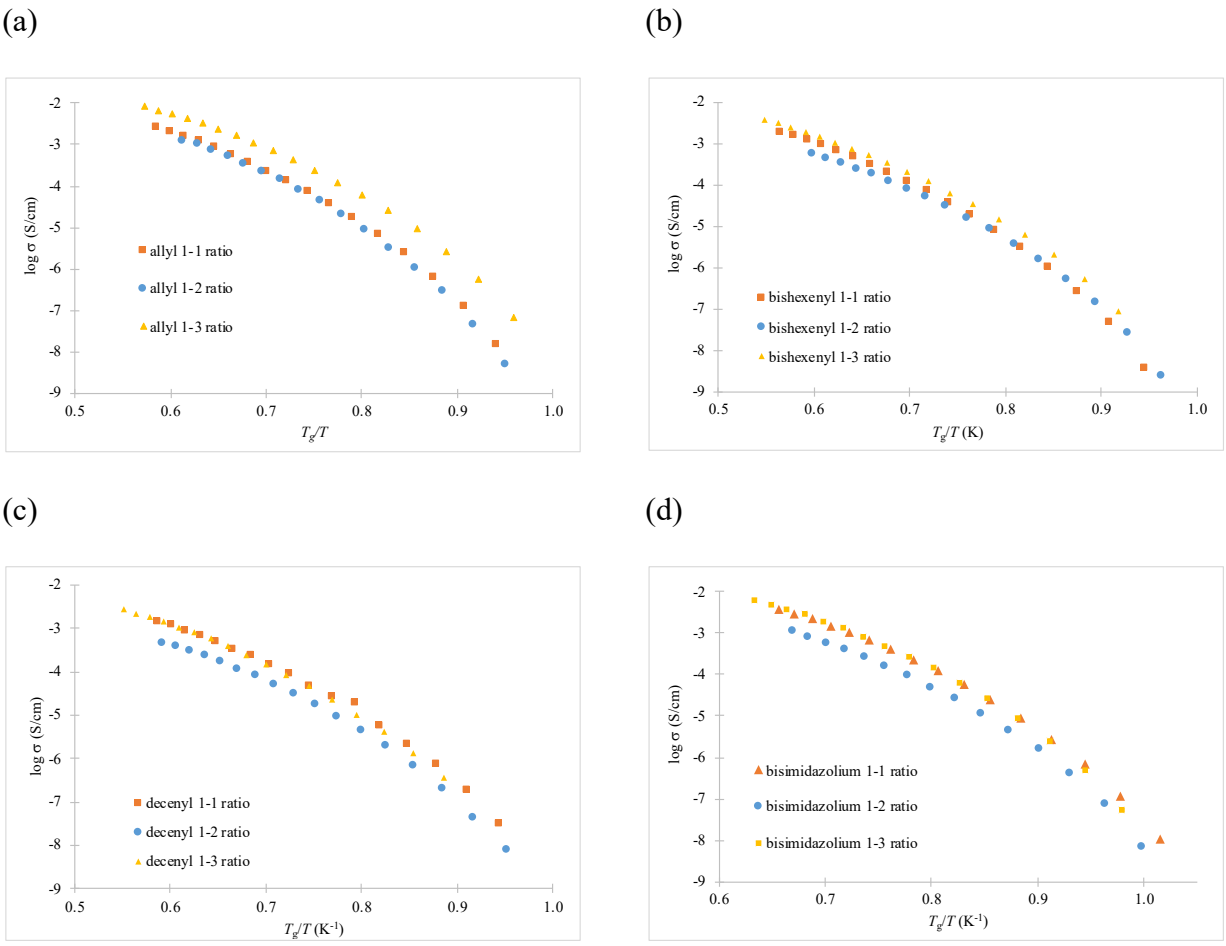

Figure 2.3. $\log(\sigma_{DC})$ vs. T_g-normalized temperature [expressed as T_g/T, both absolute temperatures in Kelvin] for the allyl (a), hexenyl (b), decenyl (c), and bisimidazolium (d).

Curiously, though, this trend in ionic conductivity by IL monomer for the 1:2 networks does not remain the same at higher temperatures. Figure 2.4, which shows a plot of these conductivities of each of the 1:2 systems as a function of temperature ($1000/T$). shows that for the monoimidazolium networks, the trend inverts above 50°C. The bisimidazolium network has a higher conductivity across the temperature range scanned, leading to a high-temperature trend of decenyl < hexenyl < allyl < bisimidazolium. The underlying reason for this trend is postulated to be that at sufficiently high temperatures, the relative T_g-dependent flexibilities of each ionene

network are less important than the networks' ion densities. This presumption makes physical sense, due to the high mechanical flexibility and relatively high ion mobility that all of the networks would be expected to experience at high temperature. Moreover, it accounts for why the bisimidazolium network remains the highest with respect to conductivity, due to its relatively high ion density and low T_g.

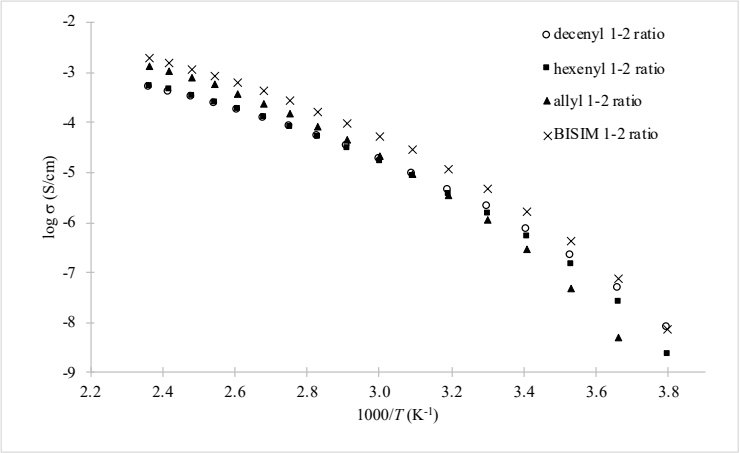

Figure 2.4. Conductivity $[\log(\sigma_{DC})]$ as a function of temperature $[1000/T]$ for each of the stoichiometric ionene networks.

The results of fitting each of the conductivity functions are parameters that mostly follow reasonably predictable trends. The values of σ_∞ follow the same trend with respect to thiol:ene molar ratio as the values of σ_{DC} at 30°C, and the trend based on IL-monomer for the ionene networks is the same as the high-temperature trend discussed in the previous paragraph, with the exception of the outlying 1:2 hexenyl system. It is presumed that this is experimental error from the high temperature end, which seems to strangely slacken its ascent with respect to the other 1:2 conductivity curves in Figure 2.4. This presumption is supported by the literature value of the 1:2 hexenyl network,[40] which fits nicely between the allyl and decenyl values as would be expected.

The Vogel temperature, T_0, correlates with the T_g's of each of the networks as theoretically expected, providing validation of the fitting parameters.

2.5. X-Ray Scattering

In order to understand the nanostructural differences in the ionene networks studied herein that might influence the conductivity trends, X-ray scattering experiments were performed on each of the networks at the University of Minnesota. The peaks observed in X-ray scattering traces are indicative of specific atomic-scale structural patterns within the material. Data from these experiments are shown by plotting signal intensity versus a parameter q, which has units of $Å^{-1}$ (inverse angstroms). Correlation lengths for each pattern are defined as $d_n = 2\pi/q_n$, where q_n is the specific value of q for that peak. The traces for the allyl, hexenyl, and decenyl networks are overlayed in Figure 2.5, along with a separate trace of the bisimidazolium system.

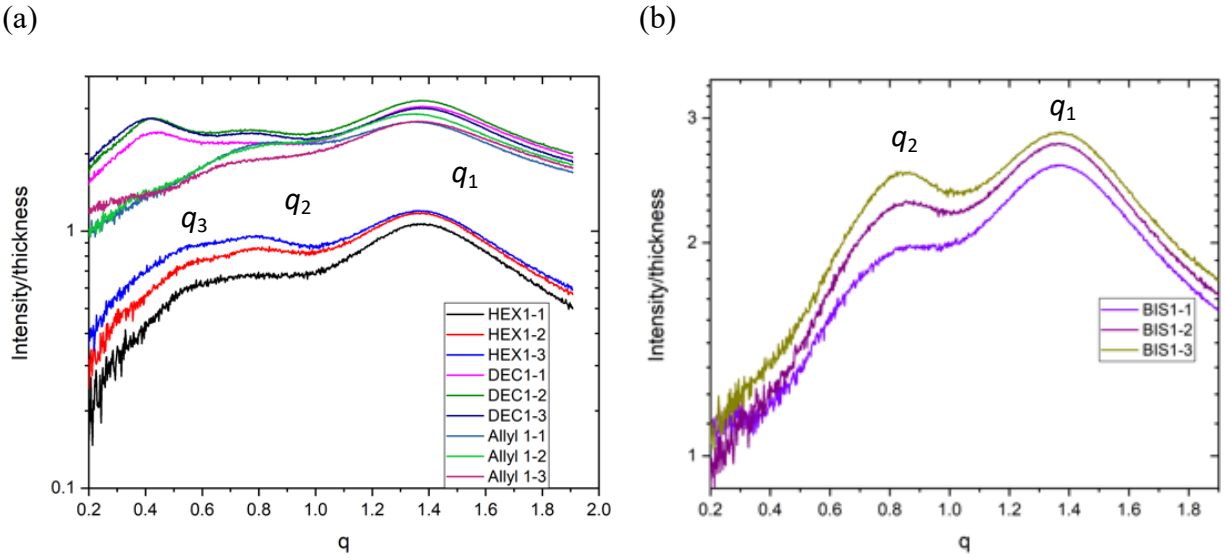

Figure 2.5. X-Ray Scattering Traces with q-peaks assigned. The allyl, hexenyl, and decenyl systems are shown in (a), and the bisimidazolium systems are shown in (b).

Two wide angle scattering peaks were assigned. The first peak, q_1 ~1.4 Å^{-1} (d_1 ~4.5 Å), is assigned to be an amorphous halo.[36] Several nanostructural features contribute to the amorphous halo, such as π-π interactions between close imidazolium rings, van der Waals interactions between alkyl chains, and other intermolecular interactions. The second peak, q_2 ~0.8 Å^{-1} (d_1 ~7.9 Å), is assigned to anion-to-anion correlation distance.[36] Between the ionene networks studied herein, no meaningful differences in these peaks were discerned, and therefore no trends are drawn.

One small angle scattering peak was also observed for some of the ionene networks, found at q_3 ~0.4-0.5 Å^{-1} (d_1 ~13-16 Å). It is assigned to correlation between ion clusters. No significant peak is seen for the allyl or bisimidazolium networks, but a small peak is seen for the hexenyl networks, and a higher intensity peak at a slightly higher q-value is seen for the decenyl networks. This suggests that as the alkene linker is made longer, the tendency toward nanoscale ion clustering increases, with regions that are relatively nonpolar in between, and the ion clusters exist at further distances from one another.

2.6. Summary and Future Work

In summary, clear trends in the thermal, mechanical, and conductive properties were the result of modifications in polymer architecture studied herein. In particular, varying the thiol:ene molar ratio of monomers, the length of the alkyl spacer on the IL monomer, and the number of IL moieties per monomer were tied to changes in the thermal stability of each ionene network, their glass transition temperatures, their crosslink densities and storage moduli, and their conductivities as a function of temperature. These trends allow logical tunability of the network's properties to suit a specific application, and perhaps more importantly, to guide future experiments.

Of particular interest in this study is the trend in conductive properties. Namely, the fact that the low-temperature trend in conductivity (given a 1:2 thiol:ene molar ratio), allyl < hexenyl < decenyl < bisimidazolium below 50°C, differs from the high-temperature trend, decenyl < hexenyl < allyl < bisimidazolium above 50°C, suggesting that conductivity depends upon more than one structural variable, and that those variables have different degrees of effect as the temperature is increased. It is postulated that the low-temperature trend is due to the demonstrated partial dependence of the conductivity on the T_g of the ionene network. However, at high temperatures, it appears that the ion density is a predominant factor in governing the conductivity relationship between the ionene networks. This is supported from two respects: the first being the reversal of the three 1:2 monoimidazolium networks from a T_g-consistent ordering to an ion density-consistent ordering, and the second being the fact that the 1:2 bisimidazolium network, which has the lowest T_g has the highest ion density of any of the 1:2 networks, has the highest conductivity over the temperature range scanned.

In future work, the Miller group hopes to strengthen the evidence for the trends apparent in this experiment. One of the possible directions for these future efforts would be to fit the DRS data to an electrode polarization model, which would allow determination of ion mobility (μ) and free ion concentration (p) for each of the ionene networks, as well as their overall contributions to the conductivity. This has been done in previous publications to help establish trends in conductivity based on the counteranion,[34, 40] and may be useful to support these experiments as well. In addition, temperature dependent XRS experiments as mentioned above would be enlightening about the contribution of nanostructural organization of ionene networks to their conductivities. If the ion clustering prevalence of the allyl and hexenyl networks grows with increasing temperature, or that of the decenyl networks is, that could suggest a reason for the

change in the conductivity trend over this temperature range. If the ion clustering shows no variation with temperature, though, that would indicate that there are other prevailing factors that cause the change in the conductivity trend.

Moreover, more bisimidazolium-type monomers need to be studied to define the structure-properties relationships within this new family of ionene networks. In future experiments, bisimidazolium-type monomers with both alkyl and ether spacers, some examples of which are shown in Figure 2.6. Determining the thermal, mechanical, conductive properties of these networks will build a firmer understanding of the ways in which polymer architecture can be used to tune an ionene network's properties to suit a specific application. Further examination of the gas separation properties of this family of ionene networks would be allow for unlocking the effect of polymer architecture on CO_2 selectivity, allowing the properties of future ionene networks to be tuned to that application.

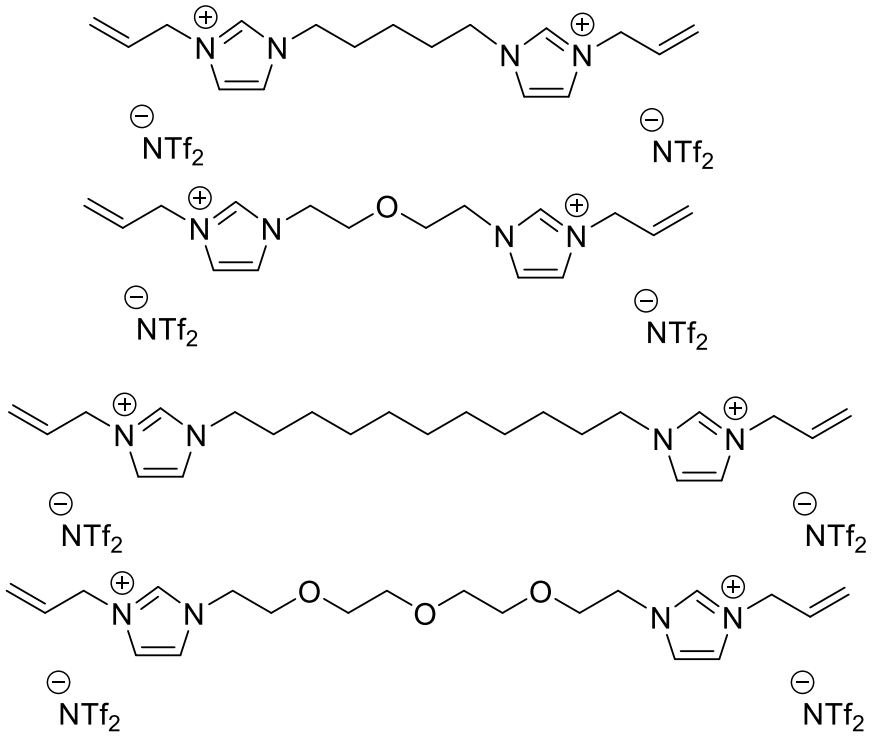

Figure 2.6. Examples of more bisimidazolium-type monomers, related to the bisimidazolium monomer used in this experiment.

Chapter 3: Experimental

3.1. Materials

All chemicals were purchased from either Sigma-Aldrich or Acros Organics and used without further purification. Sodium imidazole was synthesized via a literature method,[41] as were 1,3-bisallylimidazolium bistriflimide[37] and 1,3-bishexenylimidazolium bistriflimide.[40] Pentaerythritol tetrakis(3-mercaptopropionate) (PTMP, > 95%) was placed in a high vacuum oven (50 °C, < 0.01 mm Hg) for 48 hours prior to use. An ELGA Purelab® Ultra filtration device generated ultrapure water with a resistivity of 18 MΩ-cm.

3.2. Synthetic Procedures

Monomer Characterization: Nuclear magnetic resonance (NMR) spectra (^{1}H and ^{13}C nuclei) were recorded on a JEOL-ECS 400 MHz spectrometer, and all chemical shift values reported herein were reference to residual solvent signals ($CDCl_3$: ^{1}H, 7.240 ppm; ^{13}C, 77.184 ppm; DMSO-d_6: ^{1}H, 2.481 ppm; ^{13}C, 39.500 ppm). NMR spectra of all newly synthesized compounds are included in the Appendix section, Figures A1-A11.

Synthesis of hexane-1,6-bisimidazole: In a small round-bottomed flask charged with tetrahydrofuran (25 mL) was mixed sodium imidazole (5.010 g, 55.63 mmol) and 1,6-dibromohexane (6.095 g, 24.98 mmol) with a magnetic stir bar. The mixture was brought to reflux and held for 17 h before being allowed to cool. The solvent was then removed by rotary evaporation; the resulting crude product was added to dichloromethane (50 mL) and washed with ultrapure water (50 mL). The organic layer was isolated, dried over magnesium sulfate, filtered,

and isolated by rotary evaporation to yield a yellow oil (3.865 g, 70.87%). ^{1}H-NMR ($CDCl_3$, 400 MHz): δ 7.493 (s, 2H), 7.026 (s, 2H), 6.856 (s, 2H), 3.892 (t, 4H, J = 6.8 Hz), 1.726 (quint, 4H, J = 6.9 Hz), 1.257 (quint, 4H, J = 7.6 Hz).

Synthesis of hexane-1,6-bis(3-allylimidazolium bromide): To a small round-bottomed flask charged with acetonitrile (40 mL) was added hexane-1,6-bisimidazole (3.865 g, 17.71 mmol) and allyl bromide (6.500 g, 53.72 mmol, 3.03 eq.). This mixture was stirred magnetically at 65°C for 21 h, then the solvent was removed by rotary evaporation and the resulting off-white solid dried in a vacuum oven (6.895 g, 84.61%). ^{1}H-NMR (DMSO-d_6, 400 MHz): δ 9.268 (s, 2H), 7.843 (t, 2H, J = 1.8 Hz), 7.747 (t, 2H, J = 1.8 Hz), 6.039 (ddt, 2H, J = 17.2, 10.4, 6.0 Hz), 5.348 (dd, 4H, J = 10.2, 1.4 Hz), 5.265 (dd, 4H, J = 17.2, 1.2 Hz), 4.845 (d, 4H, J = 6.0 Hz), 4.172 (t, 4H, J = 3.4 Hz), 1.778 (quint, 4H, J = 7.0 Hz), 1.249 (quint, 4H, J = 7.2 Hz). ^{13}C-NMR (DMSO-d_6, 100 MHz): δ 136.076, 131.795, 122.594, 122.556, 120.172, 50.856, 48.749, 29.069, 24.874.

Synthesis of hexane-1,6-bis(3-allylimidazolium bis(trifluoromethane)sulfonimide): In a large round-bottomed flask, hexane-1,6-bis(3-allylimidazolium) bromide (6.390 g, 13.86 mmol) was added to a solution of lithium bis(trifluoromethane)sulfonimide (8.640 g, 30.10 mmol, 2.168 eq.) in ultrapure water (80 mL). The mixture was stirred magnetically overnight, during which time a dense oily phase separated out. Dichloromethane (120 mL) was added, and the organic layer isolated in a separatory funnel. This organic layer was washed with ultrapure water (3x80 mL), then the solvent removed by vacuum pressure to yield a light brown oil (11.200 g, 93.88%). A few milligrams of the product were dissolved in acetone (1 mL) and mixed with a concentrated solution of silver nitrate in water (1 mL); the absence of precipitate confirmed the absence of bromide ions

in the product. ^{1}H-NMR (DMSO-d_6, 400 MHz): δ 9.136 (s, 2H), 7.782 (t, 2H, J = 1.8 Hz), 7.720 (t, 2H, J = 1.6 Hz), 6.028 (ddt, 2H, J = 17, 10.6, 6.0 Hz), 5.353 (dd, 4H, J = 10.2, 1.0 Hz), 5.255 (dd, 4H, J = 17.2, 1.2 Hz), 4.815 (d, 4H, J = 6.0 Hz), 4.141 (t, 4H, J = 7.4 Hz), 1.769 (quint, 4H, J = 6.8 Hz), 1.249 (quint, 4H, J = 3.5 Hz). ^{13}C-NMR (DMSO-d_6, 100 MHz): δ 136.047, 131.737, 122.575, 122.603, 120.163, 119.467 (q, J = 320.0 Hz, -CF_3), 50.894, 48.815, 29.088, 24.960.

Synthesis of 1-decenylimidazole: In a small round-bottomed flask charged with tetrahydrofuran (8 mL) was mixed sodium imidazole (1.690 g, 18.77 mmol) and 10-bromodecene (3.615 g, 16.49 mmol). The mixture was stirred magnetically, brought to reflux, and held for 48 h before being allowed to cool. The solvent was removed by rotary evaporation; the resulting crude orange oil (3.655 g) was loaded onto a column, through which was run hexanes with a gradient of acetone. Fractions containing correct product were combined and the solvent removed by rotary evaporation, and the resulting oil was dried in a vacuum oven for 48 h (2.345 g, 68.91%). ^{1}H-NMR ($CDCl_3$, 400 MHz): δ 7.686 (s, 1H), 7.064 (s, 1H), 6.899 (t, 1H, J = 1.4 Hz), 5.770 (ddt, 2H, J = 17.0, 10.2, 6.8 Hz), 4.957 (d, 1H, J = 17.6 Hz), 4.900 (d, 1H, J = 10.2 Hz), 3.936 (td, 2H, J = 7.2, 2.0 Hz), 2.001 (q, 2H, J = 6.8), 1.753 (quint, 2H, J = 6.8 Hz), 1.4-1.2 (m, 10H). ^{13}C-NMR ($CDCl_3$, 100 MHz): δ 139.120, 137.070, 129.243, 118.850, 114.292, 47.112, 33.792, 31.113, 29.301, 29.063, 29.006, 28.872, 26.565.

Synthesis of 1,3-bisdecenylimidazolium bromide: In a round-bottomed flask charged with acetonitrile (20 mL) was added 1-decenylimidazole (2.000 g, 9.69 mmol) and 10-bromodecene (2.300 g, 10.5 mmol). This mixture was heated to 65°C and stirred magnetically for 72 h, being monitored by NMR spectroscopy for conversion. The solvent was removed by rotary evaporation,

and the aresulting oil washed with diethyl ether (4x10 mL) before being dried in an oven to yield purified product (3.210 g, 77.84%). ^{1}H-NMR (DMSO-d_6, 400 MHz): δ 9.391 (s, 1H), 7.854 (d, 2H, J = 2.0 Hz), 5.760 (ddt, 2H, J = 17.4, 10.2, 6.4 Hz), 4.962 (dq, 2H, J = 17.0, 1.8 Hz), 4.907 (d, 2H, J = 10 Hz), 4.177 (t, 4H, J = 7.2 Hz), 1.978 (q, 4H, J = 7.1 Hz), 1.778 (quint, 4H, J = 7.2 Hz), 1.35-1.15 (m, 20H). ^{13}C-NMR (DMSO-d_6, 100 MHz): δ 138.745, 135.914, 114.623, 48.834, 33.160, 29.231, 28.650, 28.373, 28.268, 28.211, 25.427.

Synthesis of 1,3-bisdecenylimidazolium bis(trifluoromethane)sulfonimide: In a large round-bottomed flask, *N,N'*-bis(decenyl)imidazolium bromide (2.380 g, 5.593 mmol) was added to a solution of lithium bis(trifluoromethane)sulfonimide (1.79 g, 6.235 mmol, 1.115 eq.) in ultrapure water (30 mL). The mixture was stirred magnetically overnight, during which time a dense oily phase separated out. Dichloromethane (40 mL) was added, and the organic layer isolated in a separatory funnel. This organic layer was washed with ultrapure water (3x30 mL), then the solvent removed by vacuum pressure to yield a yellow oil (2.915 g, 83.29%). A few milligrams of the product were dissolved in acetone (1 mL) and mixed with a concentrated solution of silver nitrate in water (1 mL); the absence of precipitate confirmed the absence of bromide ions in the product. ^{1}H-NMR (DMSO-d_6, 400 MHz): δ 9.166 (s, 1H), 7.777 (d, 2H, J = 2.0 Hz), 5.761 (ddt, 2H, J = 17.2, 10.0, 6.8 Hz), 4.966 (dq, 2H, J = 17.0, 1.8 Hz), 4.915 (d, 2H, J = 10.0 Hz), 4.129 (t, 4H, J = 7.0 Hz), 1.979 (q, 4H, J = 6.9 Hz), 1.759 (quint, 4H, J = 7.2 Hz), 1.35-1.15 (m, 20H). ^{13}C-NMR (DMSO-d_6, 100 MHz): δ 138.726, 135.942, 122.441, 122.460, 120.167 (q, J = 320.4 Hz, -CF_3), 114.632, 48.768, 33.131, 29.222, 28.631, 28.354, 28.259, 28.192, 25.408.

Polymer Synthesis: Covalently crosslinked thiol-ene ionene networks were prepared according to previously published procedures.[36, 37] Networks were prepared with thiol:ene monomer ratios of 1:1, 1:2, and 1:3 for each type of IL monomer. In a dark laboratory, photoinitiator diphenyl(2,4,6-trimethylbenzoyl)phosphine oxide (TPO, 1 wt%) was mostly dissolved in pentaerythritol tetrakis(3-mercaptopropionate (PTMP, 1.0 eq), with mild heating employed. The appropriate IL monomer was added (1.0, 2.0, or 3.0 eq.), then the mixture was homogenized, including complete dissolution of the photoinitiator, and injected with a small syringe between two glass slides treated with Rain-X®, spaced with a 500 μm Teflon spacer and clamped together with binder clips. Each film was then cured using a UVP Blak-Ray™ B-100 AP High Intensity UV lamp and irradiated for 5 minutes on each side. The resulting polymer network films were dried in a vacuum oven (60°C, <0.01 mmHg) for over 24 hours prior to use.

3.3. Polymer Characterization

Gel Fraction Analysis: Gel fraction and swelling data were obtained by cutting small pieces (50-100 mg) of polymer film and placing them in a cellulose thimble loaded in a Soxhlet extractor. Tetrahydrofuran solvent was flushed through the Soxhlet at reflux, and the extraction took place over the course of 24-48 hours, and swollen masses were obtained directly after removing the strip from the thimble. The strips were all allowed to dry for over 48 hours in a vacuum oven, and gel fraction masses were obtained.

Thermal and Mechanical Analysis: A TA Instruments Q200 differential scanning calorimeter (DSC) was used to determine glass transition temperatures. A small sample (5 mg) of each ionene network was cut for DSC. These samples were each sealed in a fresh aluminum hermetic pan,

heated, cooled, and then reheated, each step over a temperature range of -90°C – 150°C, with a heating rate of 5.0°C/min with nitrogen flow (40 mL/min). Glass transition temperatures were recorded for the inflection point during the second heating step. Thermal stability was evaluated for each ionene network by determining the temperature at which 5% of the polymer has decomposed; using a TA Instruments Q500 thermogravimetric analyzer (TGA), small samples (5 mg) were loaded onto a platinum pan and heated to 800°C at a rate of 5.0°C/min with continuous dry nitrogen flow (sample flow rate: 60 mL/min). The platinum pan was cleaned by discarding the bulk of the previous run's material, then burning any minor residues with a propane torch between experiments. The mechanical properties of each ionene network were found using a TA Instruments Q800 Dynamic Mechanical Analyzer (DMA). Rectangular strips were cut and run with a single frequency of 1 Hz, an amplitude of 1μm, and a heating rate of 5°C/min over a temperature range of -90.0 to 150.0°C in film tension mode.

Dielectric Relaxation Spectroscopy: Anhydrous ionic conductivity measurements were recorded on a TA Instruments DHR-2 discovery hybrid rheometer with a dielectric accessory and a Keysight Technologies E4980AL/120 LCR meter was utilized. Prior to each experiment, the sample was dried in a vacuum oven (60°C, <0.01 mmHg). A sample with approximate thickness of 500 μm was cut to fit between two 25 mm stainless steel parallel plate electrodes of the dielectric accessory, and the environmental chamber under, an atmosphere of dry nitrogen and cooled with liquid nitrogen, was closed off from its surroundings. Dielectric permittivity and conductivity were measured with an ac amplitude of ±0.01 V in 10°C steps over a frequency range of 20.0-10^6 Hz. Samples were kept with a constant axial force of 5.0 ± 0.2 N and allowed to equilibrate at each temperature for 45 min before measurements were recorded. The DC conductivity (σ_{DC}) was

determined from the plateau value observed in the frequency-dependent spectrum of the real conductivity ($\sigma' = \omega\varepsilon''\varepsilon_0$, where ω is the frequency, ε'' is the dielectric loss, and ε_0 is the vacuum permittivity).

Wide-Angle X-Ray Scattering: Temperature-dependent X-ray scattering experiments were performed in transmission mode on a Ganesha 300 XL SAXS system (SAXSLAB) with a Linkam HFS 350 variable temperature stage (Linkam Instruments) and a TMS94 liquid nitrogen pump to stabilize the temperature under a constant flow of nitrogen. Before each measurement was recorded, each sample was cooled to -50°C and then heated to 50°C. The temperature of the sample was controlled by the Linkham stage from -50°C to 50°C with a step size of 10°C (heating rate: 10°C/min) and an equilibration time of 20 min before data collection (acquisition time: 5 min). The X-ray source of this laboratory-based system was a GeniX^{3D} Cu LF, a collimated X-ray beam delivery system (Xenocs), providing a microfocused beam at $\lambda = 1.54$Å. The scattering data were recorded with an EIGER R 1 M detector (Dectris).

References

1. Hallett, J. P.; Welton, T., Room-Temperature Ionic Liquids: Solvents for Synthesis and Catalysis. 2. *Chem. Rev.* **2011**, *111* (5), 3508-3576.
2. Welton, T., Ionic Liquids: A Brief History. *Biophys. Rev.* **2018,** *10* (3), 691-706.
3. Zhao, H., Review: Current Studies on Some Physical Properties of Ionic Liquids. *Phys. Chem. Liq.* **2003,** *41* (6), 545-557.
4. Lei, Z.; Chen, B.; Koo, Y. M.; MacFarlane, D. R., Introduction: Ionic Liquids. *Chem. Rev.* **2017,** *117* (10), 6633-6635.
5. Visser, A. E.; Swatloski, R. P.; Reichert, W. M.; Mayton, R.; Sheff, S.; Wierzbicki, A.; Davis, J. J. H.; Rogers, R. D., Task-Specific Ionic Liquids for the Extraction of Metal Ions from Aqueous Solutions. *Chem. Commun.* **2001,** (1), 135-136.
6. Earle, M. J.; Esperança, J. M. S. S.; Gilea, M. A.; Canongia Lopes, J. N.; Rebelo, L. P. N.; Magee, J. W.; Seddon, K. R.; Widegren, J. A., The Distillation and Volatility of Ionic Liquids. *Nature* **2006,** *439* (7078), 831-834.
7. Yuan, J.; Mecerreyes, D.; Antonietti, M., Poly(ionic liquid)s: An Update. *Prog. Polym. Sci.* **2013**, *38* (7), 1009-1036.
8. Nulwala, H.; Mirjafari, A.; Zhou, X., Ionic Liquids and Poly(ionic liquid)s for 3D Printing – A Focused Mini-Review. *Eur. Polym. J.* **2018**, *108*, 390-398.
9. Markstedt, K.; Sundberg, J.; Gatenholm, P., 3D Bioprinting of Cellulose Structures from an Ionic Liquid. *3D Print. Addit. Manuf.* **2014**, *1* (3), 115-121.
10. Green, M. D.; Long, T. E., Designing Imidazole-Based Ionic Liquids and Ionic Liquid Monomers for Emerging Technologies. *Polym. Rev.* **2009**, *49* (4), 291-314.

11. Lin, J.-H.; Liu, Y.; Zhang, Q. M., Influence of the Electrolyte Film Thickness on Charge Dynamics of Ionic Liquids in Ionic Electroactive Devices. *Macromolecules* **2012**, *45* (4), 2050-2056.

12. Bara, J. E.; O'Harra, K. E., Recent Advances in the Design of Ionenes: Toward Convergence with High-Performance Polymers. *Macromol. Chem. Phys.* **2019**, *220* (13), 1900078.

13. Kim, O.; Kim, S. J.; Park, M. J., Low-Voltage-Driven Soft Actuators. *Chem. Commun.* **2018,** *54* (39), 4895-4904.

14. Shaplov, A. S.; Vlasov, P. S.; Armand, M.; Lozinskaya, E. I.; Ponkratov, D. O.; Malyshkina, I. A.; Vidal, F.; Okatova, O. V.; Pavlov, G. M.; Wandrey, C.; Godovikov, I. A.; Vygodskii, Y. S., Design and Synthesis of New Anionic "Polymeric Ionic Liquids" with High Charge Delocalization. *Polym. Chem.* **2011**, *2* (11), 2609-2618.

15. Bernard, F. L.; dos Santos, L. M.; Schwab, M. B.; Polesso, B. B.; do Nascimento, J. F.; Einloft, S., Polyurethane-Based Poly(ionic liquid)s for CO_2 Removal from Natural Gas. *J. Appl. Polym. Sci.* **2019**, *136* (20), 47536.

16. Shaplov, A. S.; Morozova, S. M.; Lozinskaya, E. I.; Vlasov, P. S.; Gouveia, A. S. L.; Tomé, L. C.; Marrucho, I. M.; Vygodskii, Y. S., Turning into Poly(ionic liquid)s as a Tool for Polyimide Modification: Synthesis, Characterization and CO_2 Separation Properties. *Polym. Chem.* **2016**, *7* (3), 580-591.

17. Tang, J.; Tang, H.; Sun, W.; Plancher, H.; Radosz, M.; Shen, Y., Poly(ionic liquid)s: a New Material with Enhanced and Fast CO_2 Absorption. *Chem. Commun.* **2005**, (26), 3325-3327.

18. Tang, J.; Tang, H.; Sun, W.; Radosz, M.; Shen, Y., Poly(ionic liquid)s as New Materials for CO_2 Absorption. *J. Polym. Sci. A Polym. Chem.* **2005**, *43* (22), 5477-5489.

19. Tang, J.; Sun, W.; Tang, H.; Radosz, M.; Shen, Y., Enhanced CO_2 Absorption of Poly(ionic liquid)s. *Macromolecules* **2005**, *38* (6), 2037-2039.

20. Cadena, C.; Anthony, J. L.; Shah, J. K.; Morrow, T. I.; Brennecke, J. F.; Maginn, E. J., Why Is CO_2 So Soluble in Imidazolium-Based Ionic Liquids? *J. Am. Chem. Soc.* **2004**, *126* (16), 5300-5308.

21. Pham, T. H.; Olsson, J. S.; Jannasch, P., N-Spirocyclic Quaternary Ammonium Ionenes for Anion-Exchange Membranes. *J. Am. Chem. Soc.* **2017**, *139* (8), 2888-2891.

22. Schultz, A. R.; Lambert, P. M.; Chartrain, N. A.; Ruohoniemi, D. M.; Zhang, Z.; Jangu, C.; Zhang, M.; Williams, C. B.; Long, T. E., 3D Printing Phosphonium Ionic Liquid Networks with Mask Projection Microstereolithography. *ACS Macro Lett.* **2014,** *3* (11), 1205-1209.

23. Tran, T. S.; Dutta, N. K.; Choudhury, N. R., Poly(ionic liquid)-Stabilized Graphene Nanoinks for Scalable 3D Printing of Graphene Aerogels. *ACS Appl. Nano Mater.* **2020**, *3* (11), 11608-11619.

24. Gao, R.; Wang, D.; Heflin, J. R.; Long, T. E., Imidazolium Sulfonate-Containing Pentablock Copolymer–Ionic Liquid Membranes for Electroactive Actuators. *J. Mater. Chem.* **2012**, *22* (27), 13473-13476.

25. Jangu, C.; Wang, J.-H. H.; Wang, D.; Sharick, S.; Heflin, J. R.; Winey, K. I.; Colby, R. H.; Long, T. E., Well-Defined Imidazolium ABA Triblock Copolymers as Ionic-Liquid-Containing Electroactive Membranes. *Macromol. Chem. Phys.* **2014**, *215* (13), 1319-1331.

26. Tang, J.; Radosz, M.; Shen, Y., Poly(ionic liquid)s as Optically Transparent Microwave-Absorbing Materials. *Macromolecules* **2008**, *41* (2), 493-496.

27. Anderson, E. B.; Long, T. E., Imidazole- and Imidazolium-Containing Polymers for Biology and Material Science Applications. *Polymer* **2010**, *51* (12), 2447-2454.

28. Hosseinzadeh, F.; Mahkam, M.; Galehassadi, M., Synthesis and Characterization of Ionic Liquid Functionalized Polymers for Drug Delivery of an Anti-Inflammatory Drug. *Des. Monomers Polym.* **2012**, *15* (4), 379-388.

29. Kolb, H. C.; Finn, M. G.; Sharpless, K. B., Click Chemistry: Diverse Chemical Function from a Few Good Reactions. *Angew. Chem., Int. Ed.* **2001**, *40* (11), 2004-2021.

30. Hoyle, C. E.; Bowman, C. N., Thiol–Ene Click Chemistry. *Angew. Chem., Int. Ed.* **2010**, *49* (9), 1540-1573.

31. Tibbits, A. C.; Yan, Y. S.; Kloxin, C. J., Covalent Incorporation of Ionic Liquid into Ion-Conductive Networks via Thiol–Ene Photopolymerization. *Macromol. Rapid Commun.* **2017**, *38* (13), 1700113.

32. Wilts, E. M.; Long, T. E., Thiol–ene Addition Enables Tailored Synthesis of Poly(2-oxazoline)-graft-poly(vinyl pyrrolidone) Copolymers for Binder Jetting 3D Printing. *Polym. Int.* **2020**, *69* (10), 902-911.

33. Kim, S.; Miller, K. M., Synthesis and Thermal Analysis of Crosslinked Imidazolium-Containing Polyester Networks Prepared by Michael Addition Polymerization. *Polymer* **2012**, *53* (25), 5666-5674.

34. Tracy, C. A.; Adler, A. M.; Nguyen, A.; Johnson, R. D.; Miller, K. M., Covalently Crosslinked 1,2,3-Triazolium-Containing Polyester Networks: Thermal, Mechanical, and Conductive Properties. *ACS Omega* **2018**, *3* (10), 13442-13453.

35. Nguyen, A.; Rhoades, T. C.; Johnson, R. D.; Miller, K. M., Influence of Anion and Crosslink Density on the Ionic Conductivity of 1,2,3-Triazolium-Based Poly(ionic liquid) Polyester Networks. *Macromol. Chem. Phys.* **2017**, *218* (21), 1700337.
36. Bratton, A. F.; Kim, S.-S.; Ellison, C. J.; Miller, K. M., Thermomechanical and Conductive Properties of Thiol–Ene Poly(ionic liquid) Networks Containing Backbone and Pendant Imidazolium Groups. *Ind. Eng. Chem. Res.* **2018**, *57* (48), 16526-16536.
37. Rhoades, T. C.; Wistrom, J. C.; Daniel Johnson, R.; Miller, K. M., Thermal, Mechanical and Conductive Properties of Imidazolium-Containing Thiol-ene Poly(ionic liquid) Networks. *Polymer* **2016**, *100*, 1-9.
38. Sims, S. M.; Bontrager, N. C.; Whittaker, R. E.; Miller, K. M., Correlating Structure with Ionic Conductivity in Bis(phosphonium)-Containing [NTf_2] Thiol–ene Networks. *Polym. Int.* **2019**, *68* (9), 1557-1565.
39. Green, M. D.; Salas-de la Cruz, D.; Ye, Y.; Layman, J. M.; Elabd, Y. A.; Winey, K. I.; Long, T. E., Alkyl-Substituted N-Vinylimidazolium Polymerized Ionic Liquids: Thermal Properties and Ionic Conductivities. *Macromol. Chem. Phys.* **2011,** *212* (23), 2522-2528.
40. Bontrager, N. C.; Radomski, S.; Daymon, S. P.; Johnson, R. D.; Miller, K. M., Influence of Counteranion and Humidity on the Thermal, Mechanical and Conductive Properties of Covalently Crosslinked Ionenes. *Polymer* **2021,** *222*, 123641.
41. Bara, J. E., Versatile and Scalable Method for Producing N-Functionalized Imidazoles. *Ind. Eng. Chem. Res.* **2011,** *50* (24), 13614-13619.

Appendix

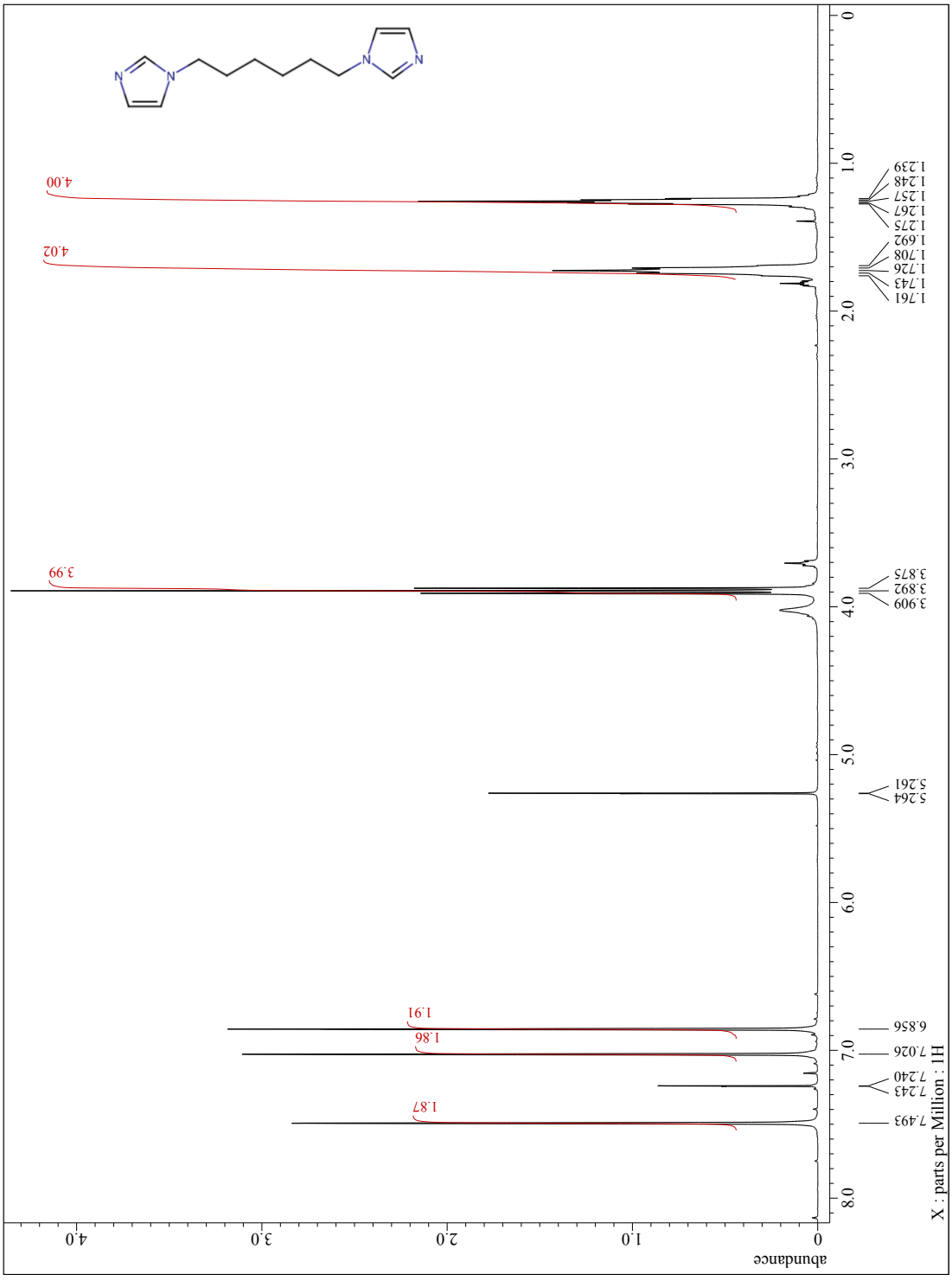

Figure A1. ^{1}H-NMR spectrum of hexane-1,6-bisimidazole ($CDCl_3$)

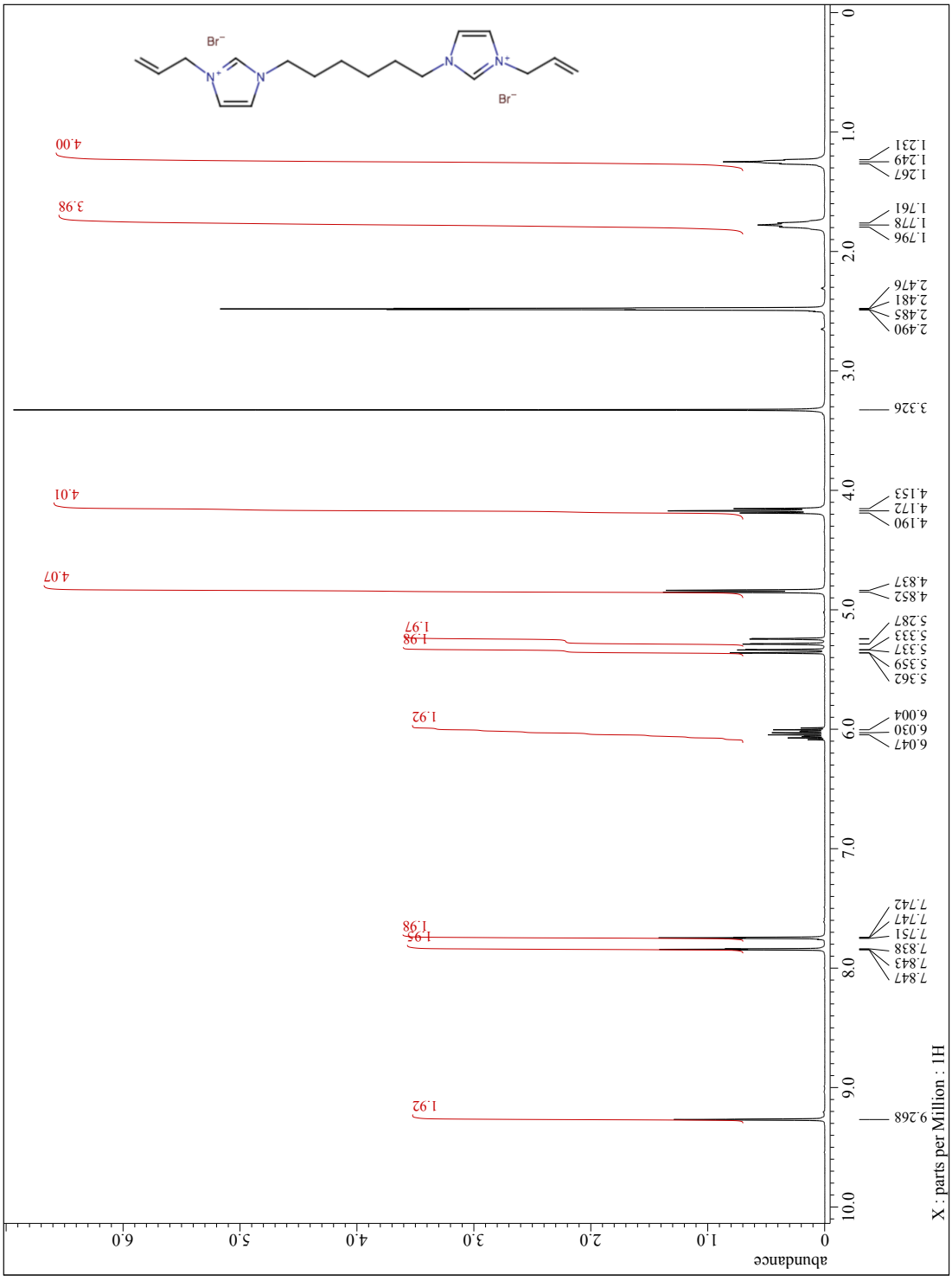

Figure A2. ^{1}H-NMR spectrum of hexane-1,6-bis(3-allylimidazolium bromide) (DMSO-d_6)

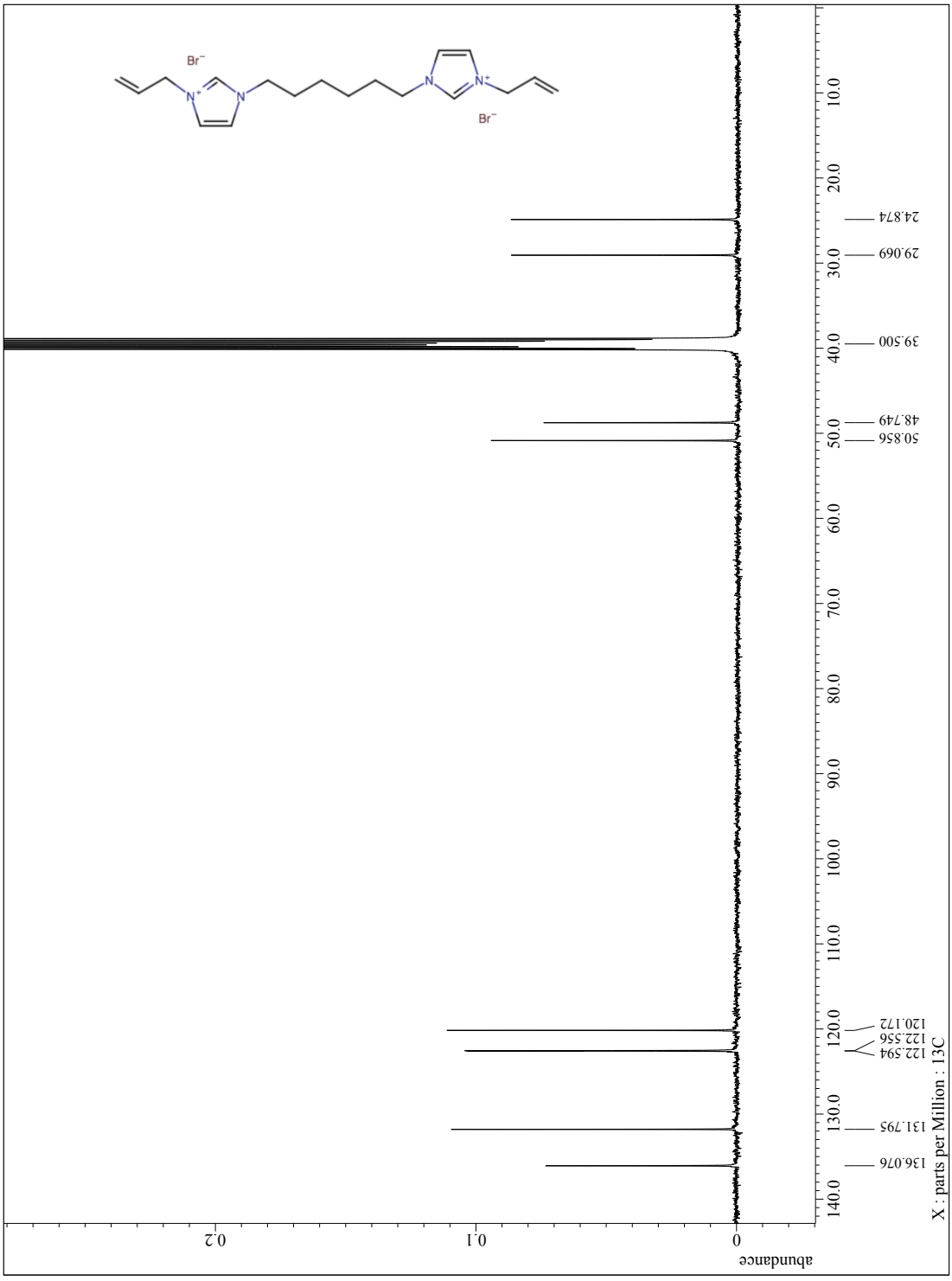

Figure A3. ^{13}C-NMR spectrum of hexane-1,6-bis(3-allylimidazolium bromide) (DMSO-d_6)

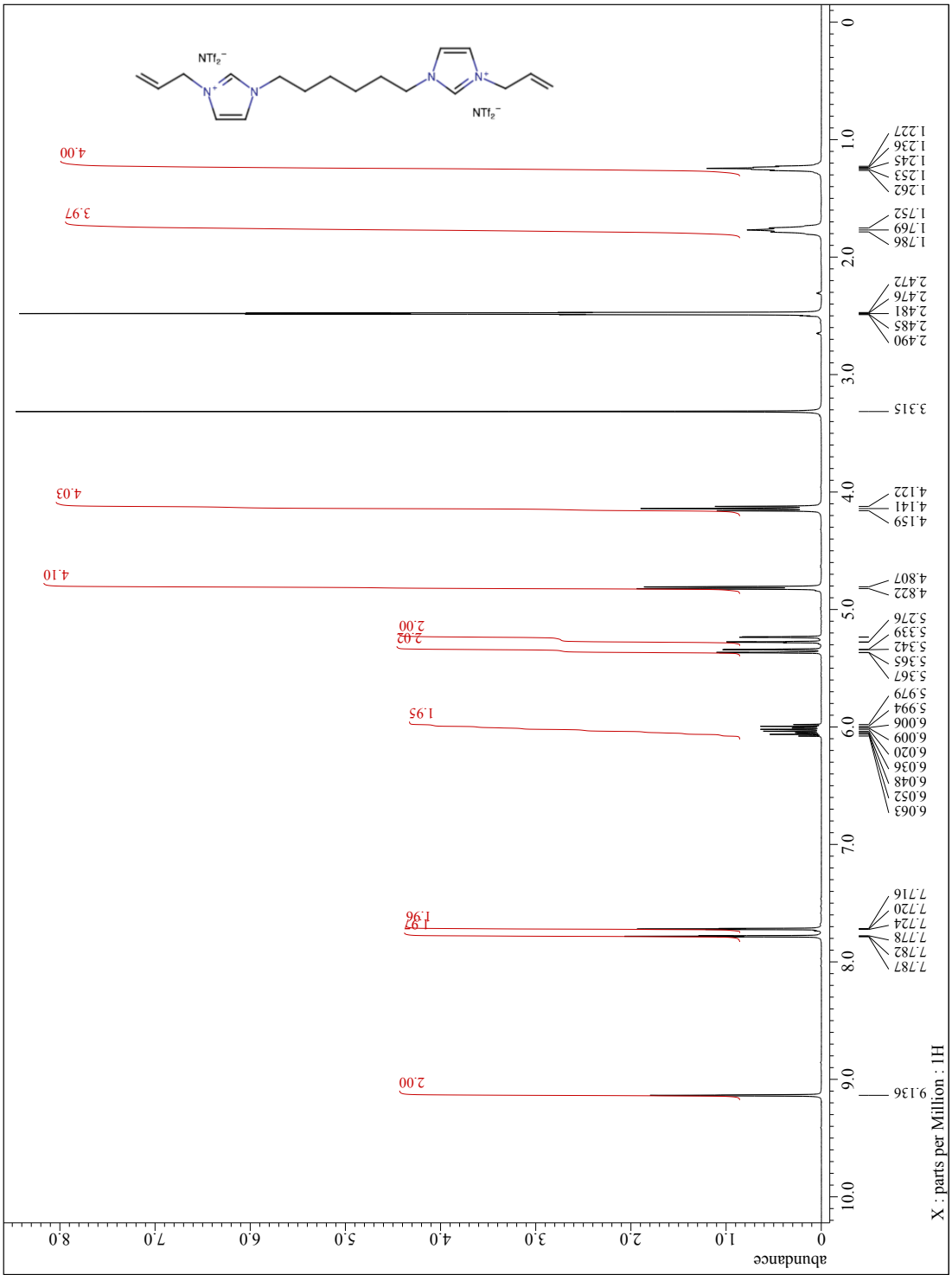

Figure A4. ^{1}H-NMR spectrum of hexane-1,6-bis(3-allylimidazolium bistriflimide) (DMSO-d_6)

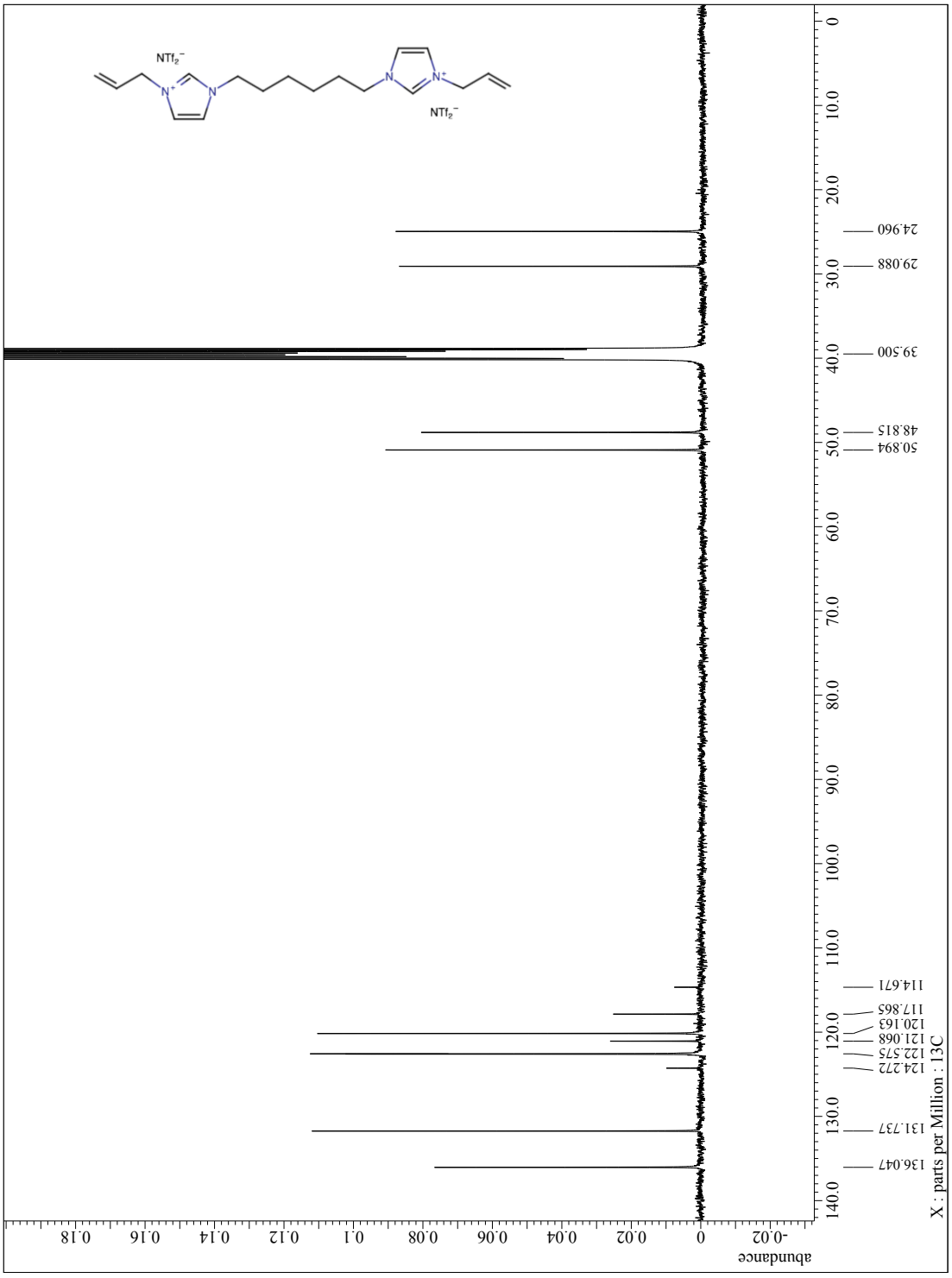

Figure A5. ^{13}C-NMR spectrum of hexane-1,6-bis(3-allylimidazolium bistriflimide) (DMSO-d_6)

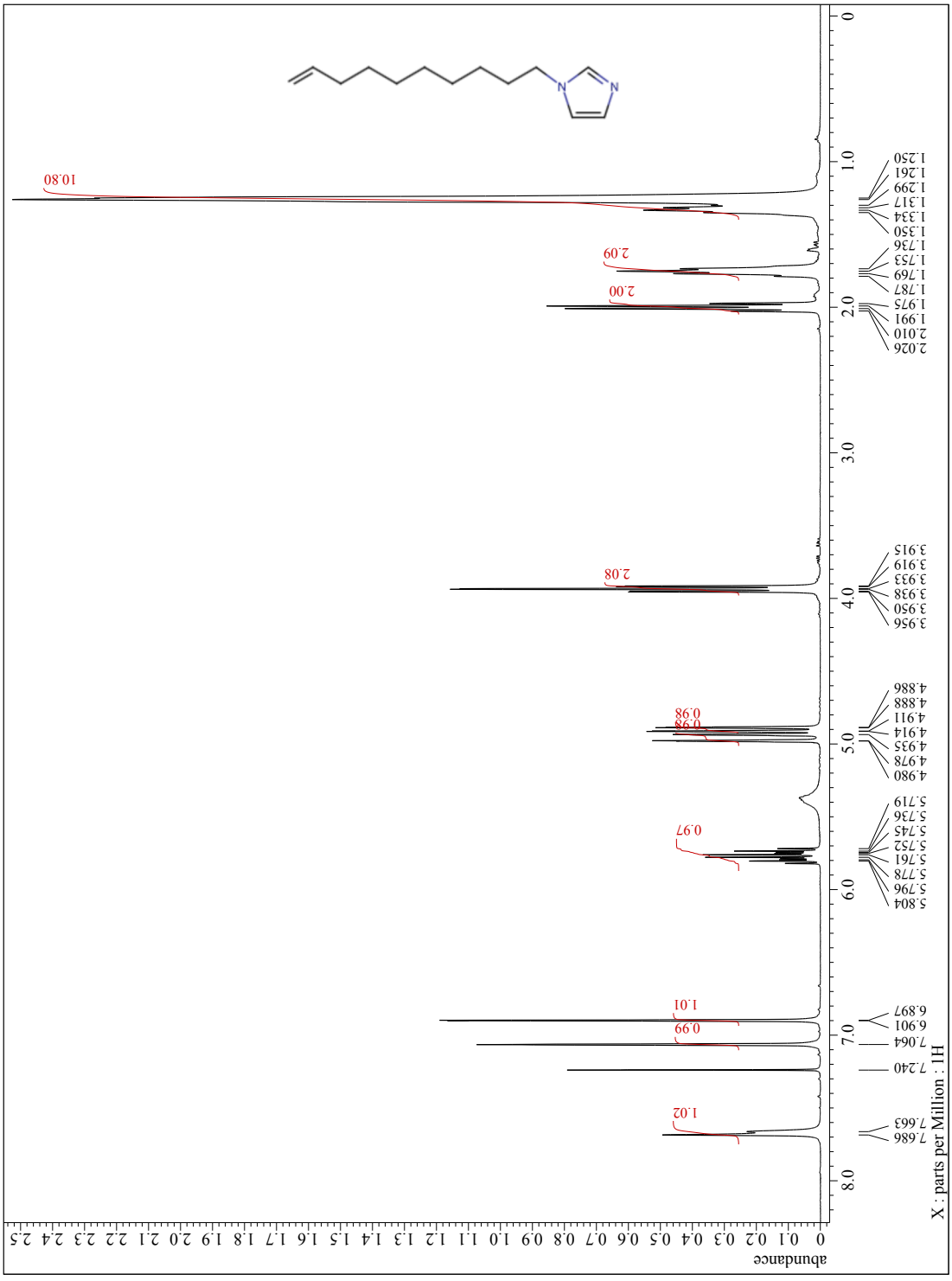

Figure A6. ^{1}H-NMR spectrum of 1-decenylimidazole ($CDCl_3$)

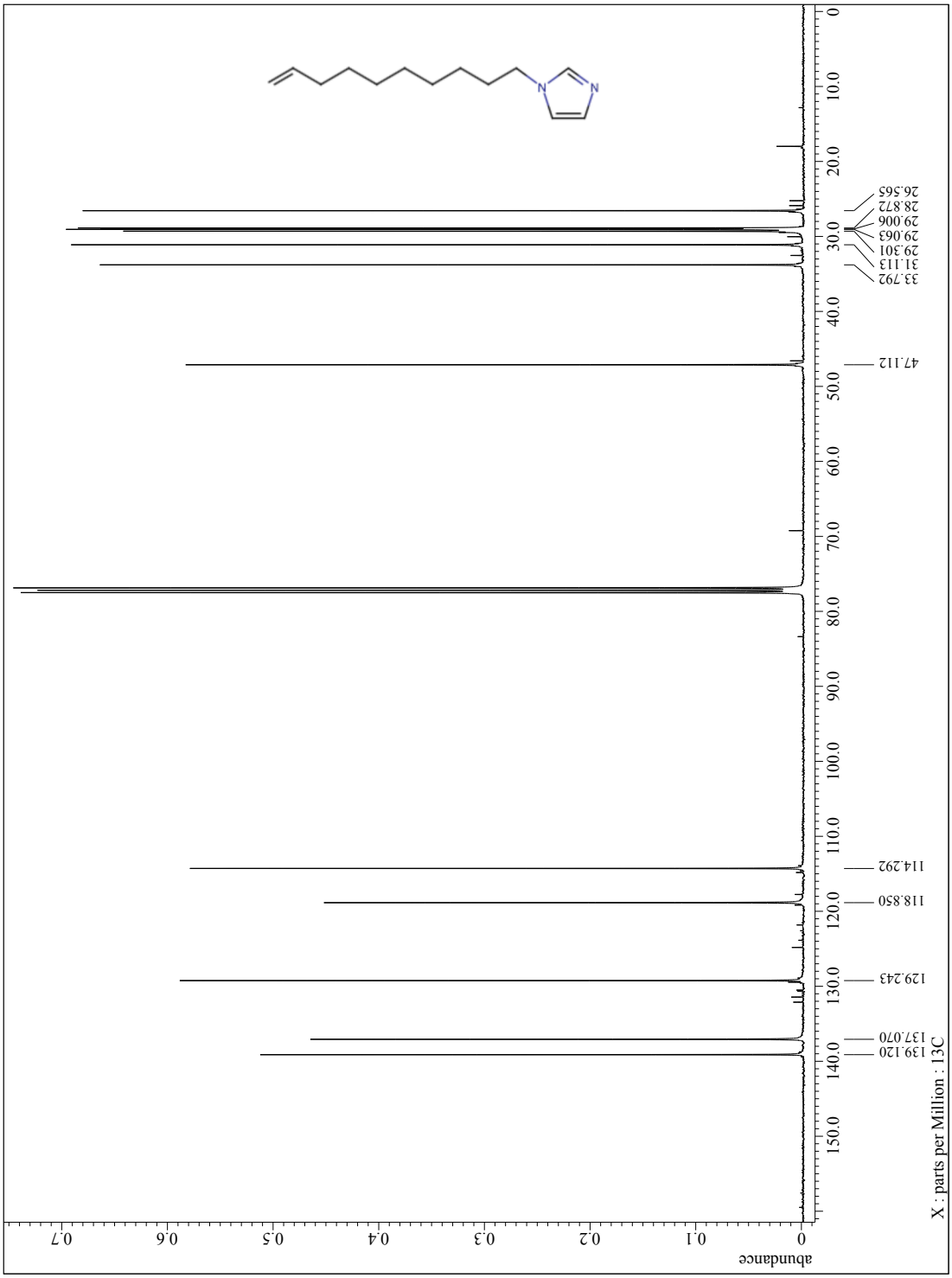

Figure A7. ^{13}C-NMR spectrum of 1-decenylimidazole ($CDCl_3$)

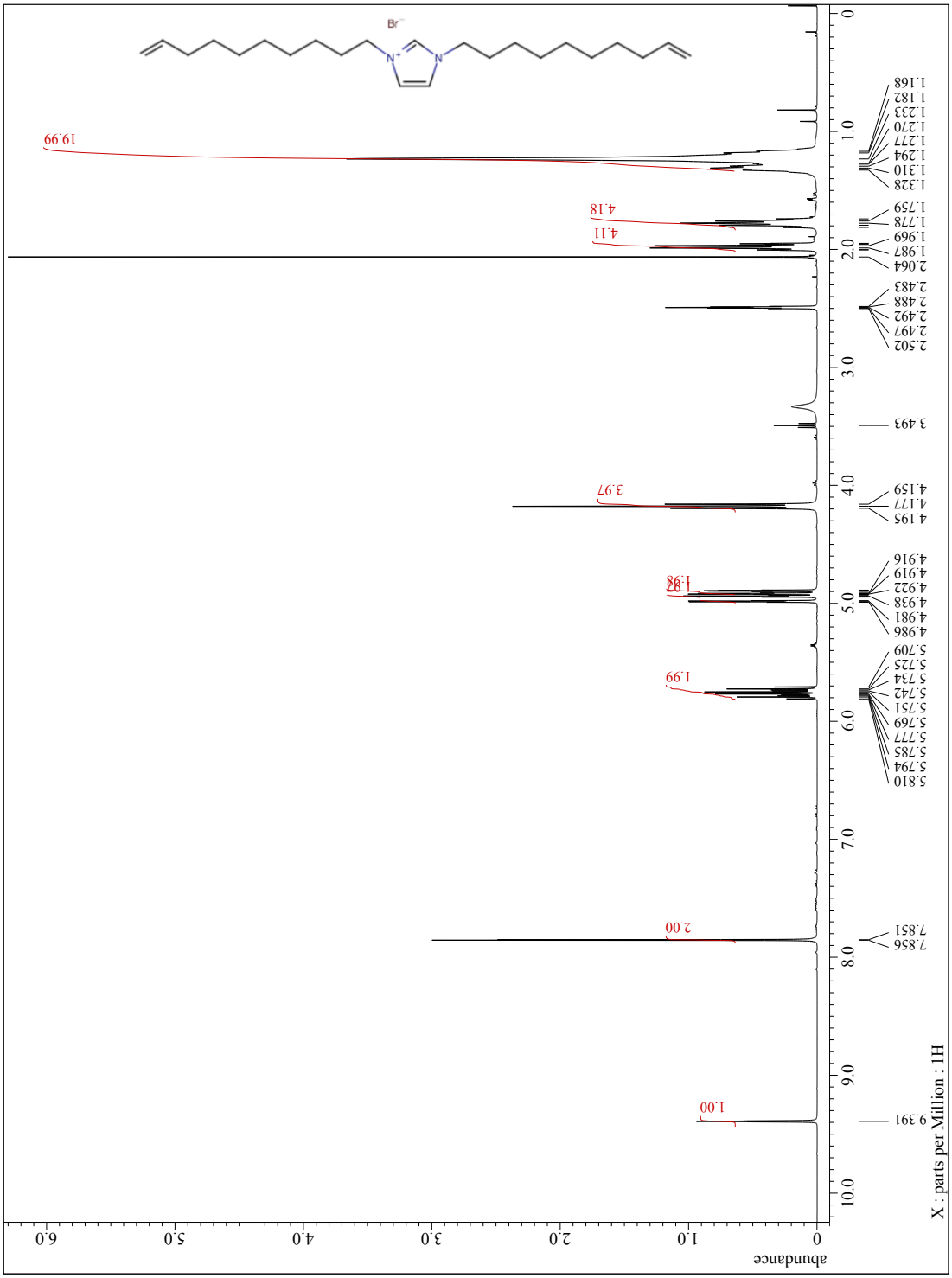

Figure A8. ^{1}H-NMR spectrum of 1,3-bisdecenylimidazolium bromide (DMSO-d_6)

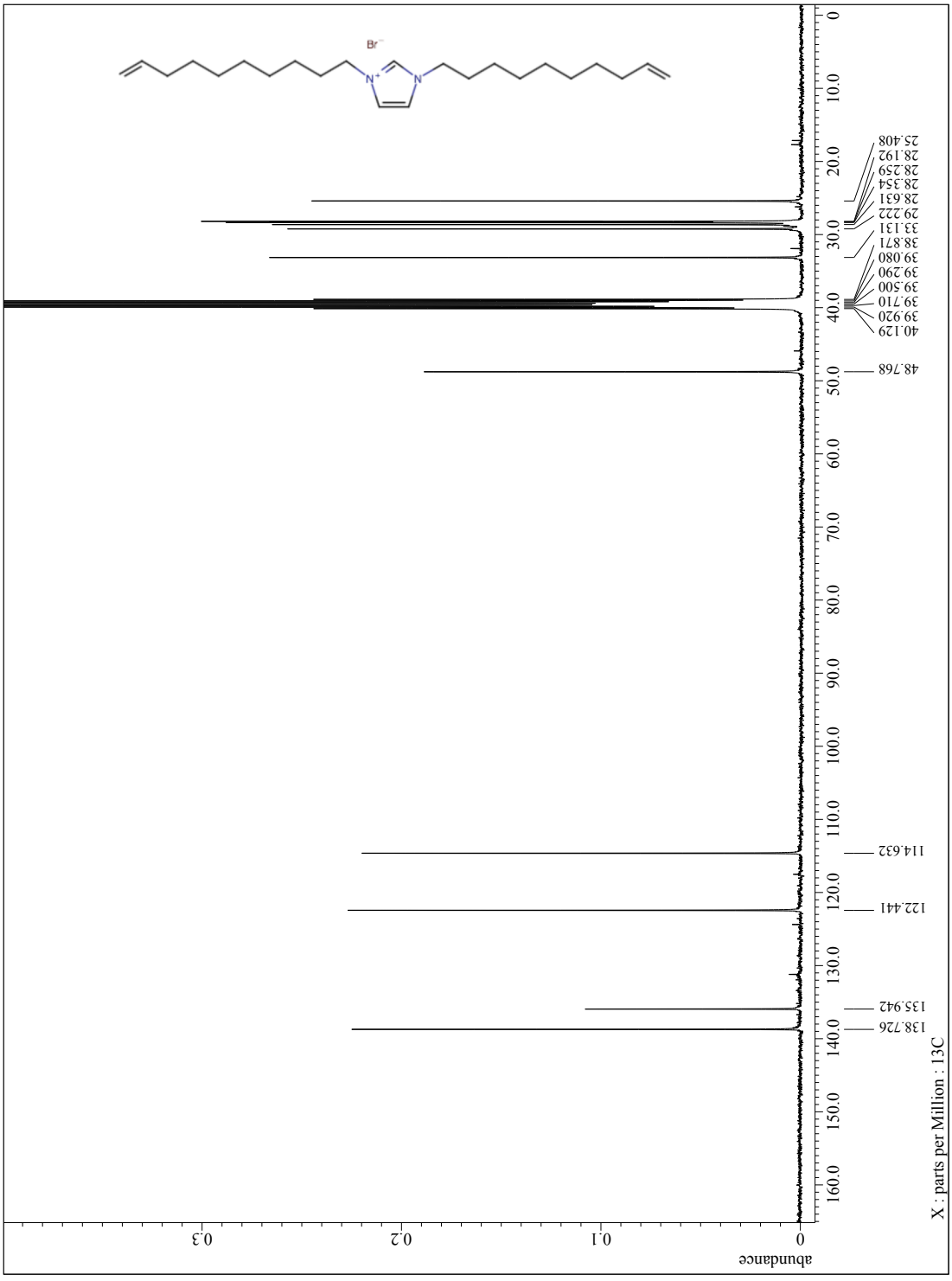

Figure A9. ^{13}C-NMR spectrum of 1,3-bisdecenylimidazolium bromide (DMSO-d_6)

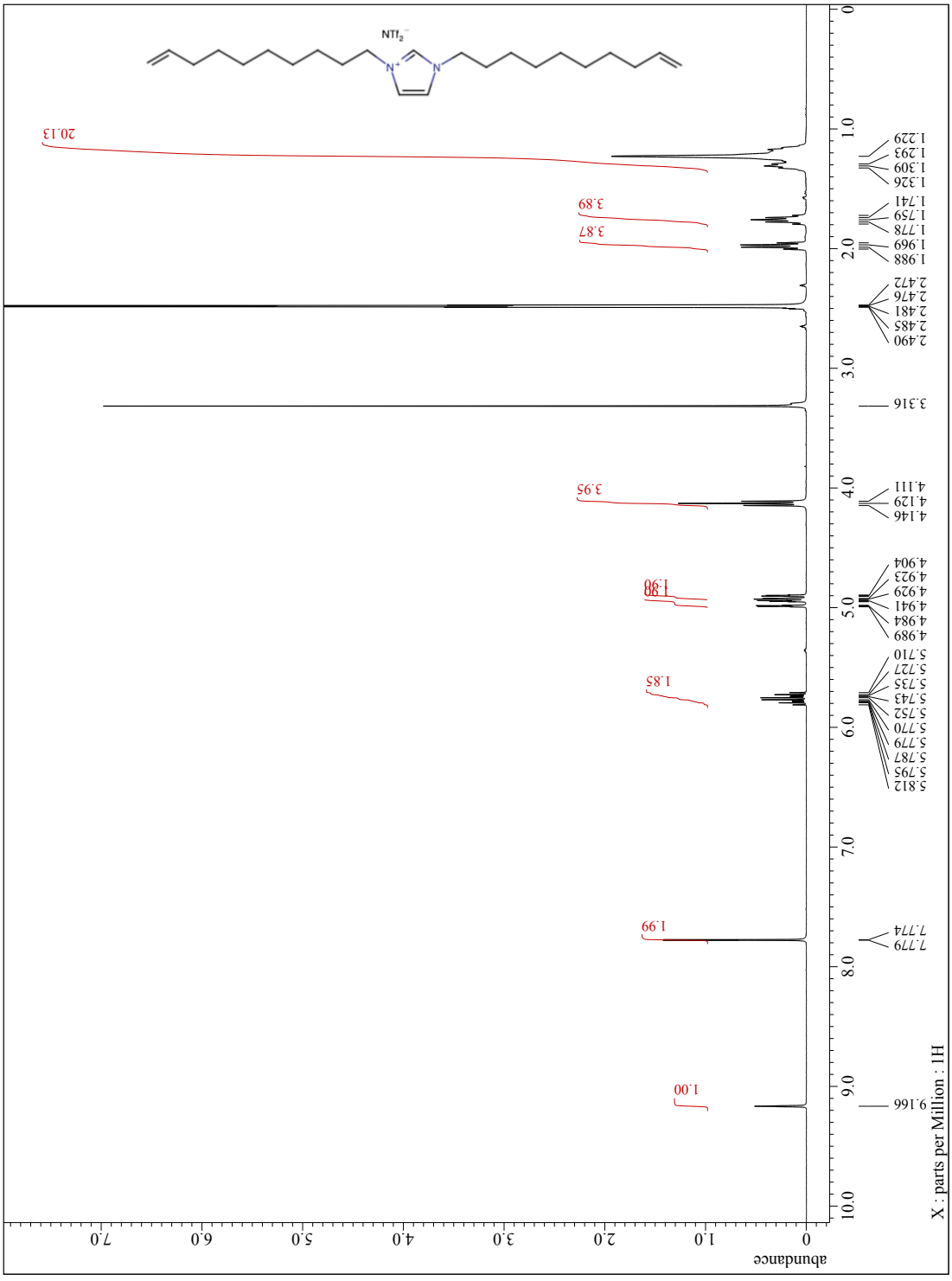

Figure A10: ^{1}H-NMR spectrum of 1,3-bisdecenylimidazolium bistriflimide (DMSO-d_6)

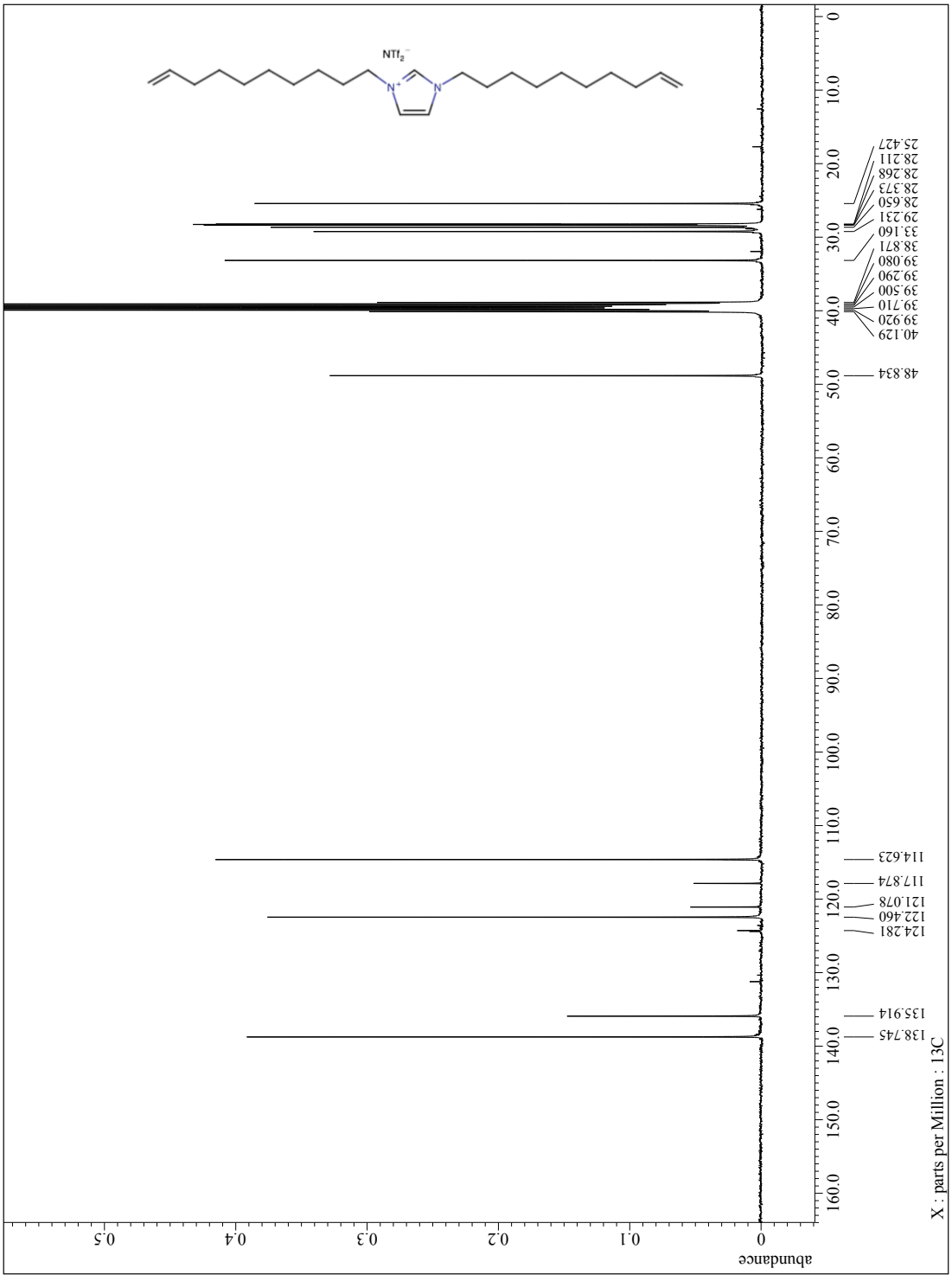

Figure A11: ^{13}C-NMR spectrum of 1,3-bisdecenylimidazolium bistriflimide (DMSO-d_6)